A novel method for high precision aortic constriction that allows for generation of specific cardiac phenotypes in mice

Arne O. Melleby[1,2,3], Andreas Romaine[1,2,3], Jan Magnus Aronsen[1,4], Ioanni Veras[1], Lili Zhang[1,2,3], Ivar Sjaastad[1,2,3], Ida G. Lunde[1,2,3], Geir Christensen[1,2,3]

[1] Institute for Experimental Medical Research, Oslo University Hospital and University of Oslo, Oslo, Norway

[2] KG Jebsen Center for Cardiac Research, University of Oslo, Oslo, Norway

[3] Center for Heart Failure Research, Oslo University Hospital, Oslo, Norway

[4] Bjørknes College, Oslo, Norway

Corresponding author:

Arne O. Melleby, Institute for Experimental Medical Research, Oslo University Hospital Ullevaal, Building 7, 4th floor, Kirkeveien 166, N-0450 Oslo, Norway.

Contact : phone +4723016800, fax: +4723016799, e-mail a.o.melleby@medisin.uio.no

Abstract

Aims: Generation of reproducible cardiac disease phenotypes in mice is instrumental for investigating mechanisms leading to heart failure. For decades, suture-based thoracic aortic constriction has been the preferred method for increasing left ventricular (LV) afterload in rodents, but the degree of stenosis resulting from this method is variable. In an effort to improve this methodology, we subjected mice to constriction of the ascending aorta using o-rings with fixed inner diameters (IDs).

Methods and Results: Mice of C57BL/6J and FVB/N background were subjected to constriction of the ascending aorta using o-rings with fixed IDs of 0.71, 0.66 and 0.61 mm. O-ring aortic banding (ORAB) resulted in 98.7% survival 2 weeks post-surgery, with very low intra- and inter-surgeon variation. When using the narrowest o-ring (0.61 mm), mice developed hypertrophy within one week. Over 20 weeks, the mice gradually developed reduced LV ejection fraction and dilatation with increased left atrial dimensions and lung weight, indicating congestion. When using o-rings with IDs of 0.66 mm and 0.71 mm, the mice developed hypertrophy, but maintained a compensated state with stabilized LV ejection fraction 8-20 weeks post-surgery. The up-regulation of signature genes associated with heart failure, hypertrophy, fibrosis and the level of activation of MAPK and NFAT signaling pathways corresponded to the degree of stenosis.

Conclusion: We here introduce a novel method for high precision aortic constriction in mice with high intra- and inter-surgeon reproducibility and low post-operative mortality that allows generation of specific cardiac disease phenotypes.

47 **Introduction**

48 Chronically elevated left ventricular (LV) afterload is one of the leading causes of heart failure (HF), and
49 is associated with high morbidity, mortality and societal costs[1,2]. Thus, new therapeutic options are sorely
50 needed. Increased understanding of the mechanisms underlying pathological cardiac remodeling is central
51 to the development of novel HF therapies[3], and reproducible *in vivo* experimental systems that allow for
52 thorough exploration of mechanisms are required[4,5].

53 Surgically-induced HF models are widely used in cardiac research. For decades suture-based
54 thoracic aortic constriction (TAC) has been the preferred method for increasing LV afterload in rodents.
55 The procedure, first described by Rockman and colleagues in 1991[6], has provided invaluable insight into
56 the underlying molecular mechanisms governing cardiac remodeling and failure and, in combination with
57 genetically modified animals, has been instrumental for mapping the role of central molecular players.

58 Reproducibility is in high demand and expected in cardiac research[4]. Suture-based TAC has
59 produced variability in LV remodeling and dysfunction leading to subgroups of failing and compensated
60 cardiac phenotypes[7-10]. For instance, suture-based TAC using a 27G needle in C57BL/6J mice results in
61 increased LV mass varying from 42% to 376% 8-9 weeks after surgery[11,12]. Moreover, mortality rates vary
62 substantially, i.e. <25%[13-16], 25-50%[17-19], and 50-75%[7,20,21]. Such variations obviously complicate and
63 confound the interpretation of mechanistic data.

64 Dissection of the specific mechanisms underlying development of clinically relevant cardiac
65 phenotypes resulting from increased LV afterload, such as HF with reduced ejection fraction (HFrEF) and
66 compensated hypertrophy, rely on precise animal models mimicking those disease states. Generation of
67 improved models would therefore represent major steps forward in the field. Thus, our aim was to develop
68 a method for highly reproducible, precise aortic constriction in mice to generate more predictable cardiac
69 remodeling and disease progression. We subjected mice to constriction of the ascending aorta using o-
70 rings with fixed inner diameters (IDs), i.e. o-ring aortic banding (ORAB).

71 **Methods**

72 **Ethics**

73 Mouse experiments were performed in agreement with the Guide for the Care and Use of Laboratory
74 Animals (NIH publication No. 85-23, revised 2011, US) and approved by the Norwegian National Animal
75 Research Committee (approval #8041 and #8617). The reporting of experimental procedures and results
76 were performed in accordance with the ARRIVE guidelines[22].

77

78 **Experimental animals**

79 Male, 9-week-old (23.5±0.1 g) C57BL/6J mice (Janvier Labs, Le Genest-Saint-Isle, France) and 8-10
80 weeks old FVB/N (24.6±0.4 g) male NFAT-luciferase reporter (NFAT-luc) mice were randomized for
81 sham, sham with inserted nitrile rubber piece (sham rub), or ORAB with IDs of 0.71 mm (ORAB 0.71),
82 0.66 mm (ORAB 0.66) or 0.61 mm (ORAB 0.61). The o-ring sizes chosen for the study were determined
83 based on echocardiographic assessment of the C57BL/6J aortic diameter and supplied by Apple Rubber
84 (Lancaster, NY). NFAT-luc mice were kindly provided by Dr. Jeffery D. Molkentin (Cincinnati
85 Children`s Hospital Medical Center, Cincinnati, OH), and carry nine copies of the NFAT-binding site
86 from the interleukin-4 promoter, upstream of the luciferase gene[23]. The C57BL/6J mice were followed for
87 2 (n=43), 4 (n=51) or 20 weeks (n=49). A cohort of C57BL/6J sham rub and ORAB 0.66 animals (n=20)
88 underwent pressure-volume measurements 12 weeks post-surgery. Surgery was performed by one mouse
89 surgeon. For evaluation of inter-operator variability, a cohort of ORAB 0.61 C57BL/6J mice (n=6) was
90 operated by a second mouse surgeon and harvested 4 weeks post-surgery. Animals received pre- and post-
91 operative analgesia (6 hours post-surgery) by subcutaneous injection of 0.02 mL (0.3 mg/mL)
92 buprenorphine. Additional analgesics were administered subject to animal status. Mice were housed in
93 cages of 6 animals per cage with *ad libitum* supply of food and water under 12/12 hour light/dark cycles.
94 At the end of experiments, hearts and lungs were weighed before the hearts were cut at the transverse
95 midventricular plane. The basal bi-ventricular part was used for histology, while the apical part of the LV

96 was snap-frozen in liquid nitrogen and stored for RNA or protein analyses. Whole LVs from NFAT-luc
97 mice (n=41) were assessed for luciferase activity 2 weeks post-surgery. Tibias were measured for organ
98 weight normalization.
99

100 **ORAB for induction of pressure overload in mice**

101 O-rings were prepared for operations by opening the ring with a lateral cut (Fig. 1A and Supplemental Fig.
102 1A) before a non-absorbable 6-0 suture (VS-802, Covidien/Medtronic, Dublin, Ireland) was thread
103 through the resulting ends at a parallel angle to the opening cut (Supplemental Fig. 1B). Suture (1.5-2 cm)
104 was left on each side of the ring ends. Mice were intubated and ventilated, breathing 98% oxygen and 2%
105 isoflurane. While fixed in the supine position on top of a heating pad, a 1-1.5 cm longitudinal incision in
106 the skin on the left side of the thorax was made using blunt scissors. After retracting the major and minor
107 pectoral muscles, the 3rd intercostal muscle was pierced using a blunt strong curved iris forceps and the
108 resulting passage was expanded by a pair of ball tip scissors. The ascending aorta was accessed by
109 retracting the costae and the thymus. Fat surrounding the aorta was trimmed away using ring tip forceps to
110 reduce variation in the degree of constriction. The suture ends from the same side of the open ring were
111 passed under the aorta using modified spinal cord hook (Supplemental Fig. 1C). Sutures, on both sides of
112 the aorta (Fig. 1A), were grasped and pulled to open the o-ring and place it around the aorta (Fig. 1B). The
113 lower and upper sutures were tied separately with two sets of overhand knots, thereby forcing the o-ring to
114 close (Fig. 1C). Excess suture was cut (Fig. 1D) and the lungs were inflated to avoid pneumothorax. The
115 residing incision was covered by the pectoral muscles, and the skin was closed with continuous sutures.
116 Animals were kept on ventilation until commencing of voluntary breathing. A video of the procedure can
117 be found in the Supplemental Material.

118 Sham-operated animals were subjected to the same operation, but without insertion of an o-ring. Sham rub
119 animals received a small piece of nitrile rubber on top of the aorta to control for possible effects of nitrile
120 rubber. The average operation time for ORAB was 12±1 minutes, sham-surgery was conducted in 8±1

121 minutes.

122

123 **Echocardiography and magnetic resonance imaging (MRI)**

124 Echocardiographic assessment of LV dimensions in diastole and systole (i.e. wall thicknesses and ID) and
125 left atrium diameter (LAD) were performed by an experienced researcher blinded to group in lightly
126 anesthetized mice breathing 1.75% isoflurane through a mask, using the VEVO 2100 (VisualSonics,
127 Toronto, Canada)[24]. Doppler-imaging of pre- and post-stenotic maximal flow velocities were captured 24
128 hours post-surgery and trans-stenotic pressure gradients were calculated using the Simplified Bernoulli
129 equation ($\Delta P=4(v_{post}^2 - v_{pre}^2)$). v_{pre}^2 was not included when lower than 1.5 m/s in accordance with previous
130 recommendations[25]. The 9.4T MRI system (Agilent, Palo Alto, CA) with a 35 mm quadrature driven
131 birdcage RF coil (Rapid Biomedical, Rimpar, Germany) was used by an experienced researcher blinded to
132 group for assessment of LV mass, LV end-diastolic volume (LVEDV), LV ejection fraction (LVEF), LV
133 lumen length and cardiac output (CO). Anesthesia given by mask during MRI-captures was between 1-2%
134 isoflurane, in order to maintain stable respiration and heart rate. Cine-MRI was acquired in the true short-
135 axis and the 4-chamber long-axis orientation in a cardiac and respiratory gated manner.

136

137 **Pressure-volume assessment of cardiac diastolic function**

138 LV catheterization was performed using an open-chest approach, as previously described[26]. In short, mice
139 were intubated and ventilated, and the thorax opened through the diaphragm using a cauterizer. A channel
140 was created to the LV lumen by an apical stab with a 25G needle and a 1F Millar pressure-volume
141 catheter (PVR-1045, Millar Instruments, Houston, TX) was inserted. End-diastolic pressure-volume
142 relationship (EDPVR) was calculated from pressure-volume cycles recorded in triplicates using LabVIEW
143 (National Instruments, Austin, TX) during inferior vena cava occlusion. Volume was adjusted to end-
144 diastolic and end-systolic volumes acquired from prior MRI measurements.

145

146 **Histochemistry**

147 The bi-ventricular base of the heart was rinsed in PBS and fixed in 10% formalin for a minimum of 24
148 hours. Fixed hearts were paraffin-embedded and sectioned at the mid-ventricular plane at 4 µm. Collagen
149 abundance was assessed by Masson's trichrome staining (25088, Polysciences, Inc., Warrington, PA)
150 according to the manufacturer's protocol. Stained sections were scanned and fibrosis area (%) quantified
151 by a researcher blinded to group using the ZEN 2 blue edition software (Zeiss, Jena, Germany).

152

153 **RNA isolation and quantitative real-time PCR (qRT-PCR)**

154 Total RNA was isolated from snap frozen LV tissue using the TissueLyser II (Qiagen Nordic, Oslo,
155 Norway) and RNeasy mini (74106, Qiagen), according to the manufacturer's protocol. cDNA synthesis
156 was performed using the iScript cDNA Synthesis Kit (Bio-Rad Laboratories, Inc., Hercules, CA).
157 Transcript levels were assessed using TaqMan assays (Applied Biosystems, Foster City, CA; listed in
158 Supplemental Material) on an ABI PRISM 7900HT Sequence Detection System (Applied Biosystems).
159 Results were analyzed using the Sequence Detection System 2.3 software (Applied Biosystems). mRNA
160 levels were normalized to *Rpl32* transcript values which remained stable at all time points (Supplemental
161 Fig. 2).

162

163 **Protein isolation and immunoblotting**

164 Snap-frozen LV tissue was homogenized using the TissueLyser II (Qiagen), in 1X PBS-based lysis buffer
165 essentially as described[24]. SDS-PAGE separation was performed before transfer onto PVDF membranes.
166 After incubation with primary and HRP-conjugated secondary antibodies (listed in Supplemental
167 Material), membranes were developed using ECL Prime (Amersham/GE HealthCare, Buckinghamshire,
168 UK) on the Las-4000 (Fujifilm, Tokyo, Japan). Densitometry and image processing were performed using
169 ImageJ (NIH) and Photoshop CS5.1.

170

171 **NFAT-luciferase activity**

172 Frozen, whole LVs from NFAT-luc mice were homogenized twice at 30 Hz for 100 seconds using the
173 TissueLyser II (Qiagen), as described in the Luciferase Assay System protocol (Promega, WI) and as
174 described previously[27]. Samples were kept on ice, vortexed and centrifuged at 12 000 g for 30 seconds.
175 Luminescence was quantified on the Hidex Sense Microplate Reader (Finland).

176

177 **Statistics**

178 All presented data are means ± SEM. Statistical tests were performed in GraphPad Prism 7.02 (GraphPad
179 Software, La Jolla, CA) or IBM SPSS Statistics for Windows, version 24. Statistical tests used were
180 repeated measures two-way ANOVA with Tukey's (>2 groups compared) or Sidak's (2 groups compared)
181 post-hoc test, one-way ANOVA with Bonferroni or Dunnet's C post-hoc test (dependent on Brown-
182 Forsythe test for equal variance), or Student's *t*-test. The coefficients of variation were calculated by group
183 standard deviations divided by group means multiplied by 100. *$P<0.05$ vs sham rub, †$P<0.05$ vs ORAB
184 0.71, ‡$P<0.05$ vs ORAB 0.66 were considered statistically significant.

185

186

187

188

189

190

191

192 **Results**

193 **ORAB results in negligible post-operative mortality**

194 The two-week post-operative ORAB survival rate was 98.7%, i.e. ORAB resulted in only 2 deaths from
195 152 operations. Necropsies revealed thoracic bleeding in both animals (ORAB 0.71 died at day 1, ORAB
196 0.71 died at day 13). Nine mice died before or during surgery due to complications during intubation and
197 thoracotomy (i.e. atria and lung injury). The survival rate of sham-operated animals was 100% (n=63).
198 Thus, ORAB results in negligible post-operative mortality.

199

200 **ORAB results in reproducible and graded myocardial hypertrophy**

201 The three ORAB groups showed increased LV posterior wall (LVPW) diameter compared to sham rub
202 animals 2-20 weeks post-surgery (Fig. 2A and Supplemental Table I). ORAB 0.66 and 0.61 showed
203 increased LVPW already at 1 week post-surgery. Similarly, increased interventricular septum diameter
204 (IVS) was evident in all three ORAB groups 8-20 weeks after operation, with increased IVS in ORAB
205 0.61 mice also at 1-2 weeks post-surgery (Fig. 2A and Supplemental Table I). A graded increase in LVPW
206 and IVS was observed among the ORAB groups, in accordance with the ID of the o-ring.

207 LV mass calculated from MRI was increased 1 week post-ORAB in the 0.61 and 0.66 groups,
208 whereas all three ORAB groups showed increased LV mass from 8-20 weeks post-surgery (Fig. 2B and
209 Supplemental Table II). Importantly, with reduced o-ring ID, the degree of hypertrophic remodeling was
210 increased. Finally, heart weight measured at harvest confirmed the findings from echocardiography and
211 MRI, showing increased hearts weight in the ORAB 0.66 and 0.61 groups at 2 weeks and in all groups at 4
212 and 20 weeks post-ORAB (Fig. 2C). The highest increase was observed in the ORAB 0.61, thus, ORAB
213 resulted in a reproducible and graded hypertrophic response.

214

215 **ORAB results in reproducible and graded cardiac dilatation and dysfunction**

216 LVEF decreased early in the ORAB 0.61, one week post-ORAB (Fig. 3A and Supplemental Table II) and
217 continued to decline, reaching 26% at 20 weeks post-surgery. The decompensated phenotype in ORAB
218 0.61 was associated with reduced fractional shortening (FS) (Supplemental Table I) and CO
219 (Supplemental Table II) at 8 weeks post-surgery. A decrease in LVEF was seen in the ORAB 0.71 and
220 0.66 groups at 8-20 weeks post-ORAB compared to sham rub mice, but without a continued decline
221 within this time frame (Fig. 3A and Supplemental Table II). Neither showed decreased FS (Supplemental
222 Table I) or CO (Supplemental Table II), confirming the stabilized phenotype. Thus, ORAB resulted in a
223 reproducible and graded cardiac contractile dysfunction.

224 In accordance with the gradually declining LV function of the ORAB 0.61 we observed an
225 increase in LVEDV 14-20 weeks post-surgery (Fig. 3B and Supplemental Table II), but no alterations
226 before these time points. In the ORAB 0.61 this might be explained by the early concentric narrowing of
227 the diastolic LV inner diameter (LVID) (Fig. 3C and Supplemental Table I). LV lumen length was
228 increased in all ORAB groups, but most profound in ORAB 0.61 (Fig. 3D and Supplemental Table II).
229 When combined with the relative increase in LVID seen in the ORAB 0.61 from 4-20 weeks, this
230 explained the overall dilated phenotype of this model, reflected by the increased LVEDV.

231 In agreement with the severe phenotype of the ORAB 0.61, LAD was increased from 1-20 weeks
232 post-ORAB (Fig. 3E and Supplemental Table I). Accordingly, ORAB 0.61 mice presented with increased
233 lung weight at 2 and 4 weeks, and with severely congested lungs at 20 weeks post-surgery (Fig. 3F).
234 ORAB 0.66 or 0.71 did not show a significant increase in LAD or lung weight compared to sham rub,
235 indicating that over this time course, ORAB 0.66 and 0.71 mice do not develop congestive HF.

236 To assess whether ORAB resulted in diastolic dysfunction in mice with a stabilized reduction in
237 LVEF, LV pressure-volume dynamics were assayed in ORAB 0.66 mice 12 weeks post-surgery. ORAB

238 0.66 mice had an increased EDPVR slope compared to sham rub animals (Supplemental Table III),
239 indicating increased myocardial stiffness and diastolic dysfunction.

240

241 **Signature molecules of cardiac remodeling and failure show a graded expression profile to ORAB**

242 Expression profiles of signature genes of cardiac remodeling were assayed in LVs harvested at 2, 4 and 20
243 weeks post-ORAB (Fig. 4A-C, respectively). All ORAB groups had elevated mRNA levels of natriuretic
244 peptides *Nppa* and *Nppb* compared to the sham rub 2 weeks post-surgery (Fig. 4A). In accordance with
245 the exacerbated degree of remodeling of ORAB 0.61 mice, this group had substantially higher levels of
246 *Nppa* and *Nppb* compared to the other ORAB groups. The enhanced concentric hypertrophic growth in the
247 ORAB 0.61 was supported by increased *Acta1* mRNA levels at 2 weeks. We did not detect major changes
248 in *Myh6* mRNA levels after ORAB, but observed a graded increase in *Myh7* expression, consistent with
249 the switch of myosin heavy chain isoforms during pathological cardiac hypertrophy. ORAB 0.66 and 0.71
250 mice expressed increased levels of fetal genes associated with adverse remodeling[28] supporting that the
251 observed remodeling in these groups was of a pathological nature despite lack of congestive HF.

252

253 **ORAB induces a graded fibrotic response**

254 LV fibrosis was assessed at 2, 4 and 20 weeks post-ORAB. mRNA levels of the fibrillar collagens *Col1a2*
255 and *Col3a1* were markedly increased in the ORAB 0.61 at 2-4 weeks, compared to the other groups (Fig.
256 5A-B). Transcript levels of the collagen crosslinking enzyme lysyl oxidase (*Lox*) was increased in all
257 ORAB groups compared to sham rub animals at 2 weeks, with the highest levels in the ORAB 0.61 (Fig.
258 5A), suggesting a stiffer collagen matrix. mRNA levels of transforming growth factor beta 1 (*Tgfb1*) were
259 increased in the ORAB 0.61 at 2-4 weeks post-surgery compared to sham rub animals (Fig. 5A).

260 Moreover, the transcript levels of the pro-fibrotic mediator connective tissue growth factor (*Ctgf*) was
261 higher in the ORAB 0.61 at all time-points, but also increased in the ORAB 0.66 (Fig. 5C).

262 Histological examination of heart cross sections stained for collagen protein were consistent with
263 the mRNA data, showing increased LV fibrosis in the ORAB 0.61 at all time-points (Fig. 6A-B). Some
264 fibrosis was detected in the ORAB 0.66 at 4 weeks post-surgery.

265 The more prominent fibrotic phenotype of the ORAB 0.61 was also evident from increased
266 mRNA and protein levels of the myofibroblast signature gene alpha-smooth muscle actin (*Acta2* gene
267 encoding the α-SMA protein) at 2 weeks post-ORAB (Fig. 6C).

268

269 **ORAB activates central cardiac remodeling signaling pathways and remodeling-associated**
270 **inflammation**

271 Activation of central cardiac remodeling signaling pathways was examined 2 weeks post-ORAB (Fig. 7).
272 Levels of phosphorylated ERK2 protein were increased in ORAB 0.61 mice animals compared to all the
273 other groups (Fig. 7A), while we did not detect changes in ERK1 phosphorylation. We did, however,
274 observe an increase in total ERK1 and 2 protein levels in the ORAB-operated mice, which were graded to
275 the o-ring ID. AKT activation was evident in all ORAB groups. p38 was only activated in the ORAB 0.61.
276 NFAT activation was measured by NFAT-luciferase activity in FVB/N NFAT-luc reporter mice (Fig. 7B).
277 Consistent with the exacerbated phenotype of the ORAB 0.61 seen by increased LV weight, NFAT
278 activation was increased in this group when compared to the sham rub controls. In agreement, mRNA
279 levels of the NFAT target gene *Rcan1.4* was increased in the ORAB 0.61 in wild-type C57BL/6J mice
280 (Fig. 7C). Thus, ORAB activates specific central cardiac remodeling signaling pathways subject to the
281 ORAB ID chosen.

282 As the regulation of pro-inflammatory cytokines has been shown to occur in the early stages of
283 cardiac remodeling following increased afterload[29], we measured the LV mRNA levels of tumor necrosis

284 factor alfa (*Tnf*), interleukin 1beta (*Il1b*), interleukin 6 (*Il6*) and interleukin 18 (*Il18*) 2 weeks post-ORAB
285 (Fig. 7D). mRNA levels of *Tnf*, *Il1b* and *Il18* were upregulated in ORAB 0.61 compared to sham rub,
286 whereas *Il18* transcript abundance was also increased in ORAB 0.66. *Il6* mRNA levels were higher in
287 ORAB 0.61 compared to all other groups, but also elevated in ORAB 0.66. Hence, the transcriptional
288 regulation of pro-inflammatory genes suggested that inflammation was enhanced in accordance with the
289 degree of constriction produced by the different o-rings.

290

291 **ORAB is performed with high intra- and inter-surgeon reproducibility**

292 Evaluation of the intra-operator reproducibility was performed by calculating the coefficient of variation
293 (CV) of heart weights within the sham rub and ORAB groups harvested at 2, 4 and 20 weeks post-surgery.
294 The average CV values of the measured heart weights within the ORAB groups were 10.8%, 12.2% and
295 17.0% at 2, 4 and 20 weeks, respectively, compared to 4.6%, 8.8% and 8.1% in the sham rub. Although all
296 animals were included, CV values for heart weight remained low. Thus, ORAB was performed with high
297 intra-surgeon reproducibility.

298 To examine the inter-surgeon variation of the ORAB method, ORAB 0.61 was performed by a
299 second surgeon with minimal ORAB training. Both ORAB 0.61 groups had similar increases in LV wall
300 thicknesses, LAD, heart weight and lung weight compared to sham rub animals 4 weeks post-surgery
301 (Supplemental Table IV). Consistently, LV mRNA levels of natriuretic peptides (*Nppa*, *Nppb*), *Acta1*,
302 *Myh7*, and collagens (*Col1a2* and *Col3a1*) were upregulated to a similar extent compared to sham rub
303 animals.

304

305

306

307 **Post-surgical exclusion is minimal with ORAB**

308 Degree of constriction in suture-based TAC of the ascending aorta is traditionally validated by
309 echocardiographic measurement of the post-stenotic maximal flow velocity (Vmax) 24 hours post-surgery
310 (Supplemental Fig. 3A)[27]. All ORAB-operated groups had an average post-stenotic Vmax of 4 m/s or
311 higher (Supplemental Fig. 3B). ORAB 0.66 had a higher post-stenotic Vmax compared to ORAB 0.71
312 (4.5 m/s vs. 4.1 m/s), but ORAB 0.61 did not differ from the other groups despite the tighter stenosis. The
313 same result was seen when calculating the trans-stenotic pressure gradient (Supplemental Fig. 3C). This
314 could be explained by the reduced LV function seen in the ORAB 0.61, as maximal pre-stenotic Vmax
315 and FS were lower in the ORAB 0.61 animals (Supplemental Fig. 3D-E). Given that gradients are a
316 squared function of flow, even a modest decrease in flow may lead to a significant reduction in gradient[30].
317 The ID of the o-ring was a better determinant of disease progression compared to the post-stenotic Vmax,
318 and we could include all operated animals while maintaining limited variation and reproducible cardiac
319 phenotypes.

320 Similarly, we did not exclude any mice due to adverse effects of the o-ring material, as cardiac
321 function and structural parameters (Supplemental Table V), organ weights and molecular markers
322 (Supplemental Table VI) were similar in the sham rub and sham groups.

323

324

325

326

327

328

329 **Discussion**

330 We have developed a novel method for constriction of the ascending aorta in mice using fixed diameter o-
331 rings. This technique results in highly reproducible pressure overload-induced remodeling with negligible
332 post-operative mortality. The fixed ID of the o-rings allow for standardized degrees of aortic constriction.
333 By using gradually narrower o-rings we induced a corresponding increasing degree of hypertrophic
334 remodeling, diastolic and systolic dysfunction, and congestive HF.

335 Aortic constriction as a model of chronically increased LV afterload has been one of the preferred
336 methods for studying mechanisms of cardiac disease. Although aortic constriction was performed in
337 rabbits[31], guinea pigs[32] and rats[33] before 1970, the development of suture-based TAC in mice in 1991[6]
338 allowed for chronically induced afterload in a species that could readily be genetically modified. This
339 combination has been invaluable in identifying mechanisms involved in cardiac disease. Attempts to
340 improve the surgical protocol for suture-based TAC in mice[6] have focused on reducing trauma when
341 accessing the aorta[34], rather than standardization of the stenosis. More work has been performed to find
342 good parameters for stratification and inclusion/exclusion of mice after TAC-surgery, than to improve the
343 method of constriction in itself[7,8,35,36].

344 Suture-based TAC is largely dependent on reproducible tightening of a suture around a sizing
345 needle. Even the best mouse surgeons will experience variations in stenosis diameter, leading to exclusion
346 or death. Previous studies have reported that suture-based TAC using a 27G needle resulted in inner
347 stenosis diameters ranging from ~0.3-0.6 mm[8] and ~0.2-0.55 mm[37], resulting in various degrees of
348 cardiac remodeling. Similarly, others have reported heterogeneity in cardiac phenotypes after suture-based
349 TAC with a 27G needle, where mice either maintain compensated hypertrophy or develop HF[7,9,10]. In
350 contrast, the stenosis diameter obtained with ORAB is decided by the ID of the o-ring. This limits the
351 possibility for constriction beyond the fixed ID and consequently leads to reproducible and consistent
352 cardiac remodeling and disease progression.

353 The post-operative survival rate of ORAB was 98.7%, with only two deaths from 152 operations
354 in the first two weeks post-surgery. In comparable suture-based TAC studies, the average two-week
355 survival rate is 78% after constriction of the ascending aorta[38-40] and 73% after constriction of the
356 transverse aorta[15-19,21]. The majority of these early deaths are reportedly due to acute HF, suggesting
357 excessive constriction. We believe that standardization of the constriction and avoidance of total occlusion
358 during the procedure[41] were responsible for the negligible mortality observed with ORAB.

359 Another source of variation that did not occur with ORAB was band internalization. Previous
360 studies show that the suture used for constriction can be internalized into the aortic lumen, resulting in
361 reduced stenosis and cardiac remodeling[7,37]. Lygate *et al.* reported suture internalization in 25% of TAC-
362 operated mice 4 weeks post-surgery, and showed that a broader stenosis obtained by insertion of two
363 parallel sutures abrogated this problem[37]. As the cross section of the o-rings used for ORAB is larger than
364 suture, we did not observe o-ring internalization even 20 weeks post-surgery. Moreover, the inert nitrile
365 rubber material of the o-rings did not cause any adverse effects upon insertion, in line with other studies
366 where acrylonitrile-butadiene polymers have been inserted in rats and rabbits[42,43]. Based on these traits, we
367 speculate that ORAB could also serve as an improved debanding model to study reverse remodeling.
368 Suture-based debanding models of reverse remodeling in mice do exist[44,45], however the method is rarely
369 used as the procedure must be performed frequently to maintain acceptable success rates[44]. As debanding
370 may offer insight into molecular drivers of reverse remodeling, it will be interesting to see whether ORAB
371 debanding can and will be used for this purpose in future studies.

372 ORAB allows for grading of aortic constriction, leading to distinct cardiac patho-phenotypes
373 important for studies of clinically relevant types of HF. In comparable suture-based TAC studies[14,46],
374 constriction using needles with decreasingly smaller diameter has been tested. However, the variation in
375 suture tightening resulted in relatively high mortality due to acute HF in all groups within two weeks of
376 surgery, despite the different sizing needles. With ORAB we avoided these limitations by using fixed
377 diameter o-rings with various diameters.

378 A model with transition from concentric hypertrophic remodeling to congestive, dilated HF over
379 20 weeks was produced by using o-rings with an ID of 0.61 mm. The ORAB 0.61 presented with a rapid
380 increase in LV wall thickness, reduced LVID and substantially elevated levels of natriuretic peptides and
381 pro-hypertrophic genes. Fibrotic remodeling was present 2 weeks post-surgery along with increased
382 transcription of pro-inflammatory genes. Left atrial and ventricular dilatation followed, with a doubling of
383 LVEDV and pulmonary congestion after 20 weeks. The specific mechanisms involved in transition from
384 compensatory concentric hypertrophy to congestive, dilated HF with severely impaired function (i.e.
385 HFrEF) are yet to be elucidated. ORAB 0.61 provides a new experimental *in vivo* setup to more precisely
386 study HFrEF and transition to congested HF.

387 By using o-rings with an ID of 0.66 mm, we produced a model of concentric hypertrophy with
388 progressive LV hypertrophic growth, elevated levels of natriuretic peptides, without pulmonary
389 congestion over the 20 weeks of the study. LVEF in ORAB 0.66 stabilized 4-20 weeks post-surgery. Pro-
390 hypertrophic, pro-fibrotic and pro-inflammatory genes were moderately increased. Fibrosis was present at
391 4 weeks, and increased *Ctgf* at 2, 4 and 20 weeks suggested fibrotic progression. During the time period
392 with stabilized contractile function (4-20 weeks post-surgery) LV stiffness was increased, indicating that
393 ORAB 0.66 may serve as a model for HF with mid-range reduced EF (HFmrEF), or even HF with
394 preserved EF (HFpEF). Indeed, diastolic dysfunction with stable systolic function has been difficult to
395 achieve experimentally using suture-based TAC due to the acuteness and severity of the increased
396 afterload[47,48]. Such models would be of importance for understanding molecular drivers that differ
397 between HFrEF, HFmrEF and HFpEF. By using ORAB 0.66 and ORAB 0.71 we induced hypertrophic
398 LV remodeling in mice without severely compromising systolic function.

399 Fixed diameter constrictors were introduced in guinea pigs already in the 1960s and 70s to
400 standardize the degree of stenosis[49] and have later been applied in rats, using metal clips[50]. These were
401 also tested in mice[51-53]. In contrast to suture-based TAC or ORAB, clips do not induce a circular
402 constriction as the aorta is asymmetrically distorted. Since the aorta is compressed rather than constricted,

403 the total cross-sectional area at the stenosis is difficult to control. Clips adjusted to 27, 30 and 32G needles
404 have been applied without achieving reproducible, graded cardiac remodeling and dysfunction[51-53]. We
405 therefore believe that the constriction obtained with ORAB is superior to clip-constriction with regards to
406 stenosis standardization.

407 Different mouse strains respond differently to pressure overload[13,16]. In our study, we provide
408 detailed description of the cardiac phenotype of the C57BL/6J mouse strain following ORAB, and we also
409 observed a reproducible and graded remodeling response in FVB/N mice upon ORAB. Whether the
410 phenotypes we observed are transferrable to other mouse strains remains to be investigated. Moreover,
411 age- and size-matched mice should be used for ORAB and suture-based TAC, since differences in aorta
412 diameter may influence the degree of constriction with the same o-ring or sizing needle.

413 In summary, we have developed a novel method for high precision aortic banding in mice. ORAB
414 offers high intra- and inter-surgeon reproducibility, low post-operative mortality and reproducible HF
415 phenotypes. The HF phenotypes are relevant for HFrEF, and possibly also HFpEF. We strongly believe
416 that implementation of ORAB will increase the quality and reproducibility of pre-clinical studies of HF.

417

418

419

420

421

422

423

424

Funding

This study was funded by the KG Jebsen Center for Cardiac Research; the Norwegian Health Association, the South-Eastern Regional Health Authority; the Research Council of Norway; Anders Jahre's Fund for the Promotion of Science; the Simon Fougner Hartmanns Family Fund, Denmark; and Olav Raagholt and Gerd Meidel Raagholt´s Fund for Science, Norway.

Acknowledgements

We would like to thank Dina Behmen and Monika Gelazauskaite at Oslo University Hospital for excellent technical assistance with gene expression and protein analysis, Vidar Magne Skulberg at Oslo University Hospital for technical assistance with hemodynamic measurements and Gary McGinley at Oslo University Hospital for video editing.

Conflict of interest

None declared.

446 **References**

447 1. Dunlay SM, Weston SA, Jacobsen SJ, Roger VL. Risk factors for heart failure: a population-
448 based case-control study. *Am J Med.* 2009;**122**:1023-1028.
449 2. Bui AL, Horwich TB, Fonarow GC. Epidemiology and risk profile of heart failure. *Nat Rev*
450 *Cardiol.* 2011;**8**:30-41.
451 3. Kaye DM, Krum H. Drug discovery for heart failure: a new era or the end of the pipeline? *Nat*
452 *Rev Drug Discov.* 2007;**6**:127-139.
453 4. Bolli R. New initiatives to improve the rigor and reproducibility of articles published in
454 Circulation Research. *Circ Res.* 2017;**121**:472-479.
455 5. Ramirez FD, Motazedian P, Jung RG, Di Santo P, MacDonald ZD, Moreland R, Simard T,
456 Clancy AA, Russo JJ, Welch VA, Wells GA, Hibbert B. Methodological rigor in preclinical
457 cardiovascular studies: targets to enhance reproducibility and promote research translation. *Circ*
458 *Res.* 2017;**120**:1916-1926.
459 6. Rockman HA, Ross RS, Harris AN, Knowlton KU, Steinhelper ME, Field LJ, Ross J, Chien KR.
460 Segregation of atrial-specific and inducible expression of an atrial natriuretic factor transgene in
461 an in vivo murine model of cardiac hypertrophy. *PNAS.* 1991;**88**:8277-8281.
462 7. Mohammed SF, Storlie JR, Oehler EA, Bowen LA, Korinek J, Lam CSP, Simari RD, Burnett JC,
463 Redfield MM. Variable phenotype in murine transverse aortic constriction (TAC). *Cardiovasc*
464 *Pathol.* 2012;**21**:188-198.
465 8. Wu J, You J, Li L, Ma H, Jia J, Jiang G, Chen Z, Ye Y, Gong H, Bu L, Ge J, Zou Y. Early
466 estimation of left ventricular systolic pressure and prediction of successful aortic constriction in a
467 mouse model of pressure overload by ultrasound biomicroscopy. *Ultrasound Med Biol.*
468 2012;**38**:1030-1039.
469 9. Vinet L, Rouet-Benzineb P, Marniquet X, Pellegrin N, Mangin L, Louedec L, Samuel J-L,
470 Mercadier J-J. Chronic doxycycline exposure accelerates left ventricular hypertrophy and
471 progression to heart failure in mice after thoracic aorta constriction. *Am J Physiol Heart Circ*
472 *Physiol.* 2008;**295**:H352-H360.
473 10. Kiriazis H, Sato Y, Kadambi VJ, Schmidt AG, Gerst MJ, Hoit BD, Kranias EG. Hypertrophy and
474 functional alterations in hyperdynamic phospholamban-knockout mouse hearts under chronic
475 aortic stenosis. *Cardiovasc Res.* 2002;**53**:372-381.
476 11. Lei B, Chess DJ, Keung W, O'Shea KM, Lopaschuk GD, Stanley WC. Transient activation of P38
477 MAP kinase and up-regulation of Pim-1 kinase in cardiac hypertrophy despite no activation of
478 AMPK. *J Mol Cell Cardiol.* 2008;**45**:404-410.
479 12. Takimoto E, Champion HC, Li M, Belardi D, Ren S, Rodriguez ER, Bedja D, Gabrielson KL,
480 Wang Y, Kass DA. Chronic inhibition of cyclic GMP phosphodiesterase 5A prevents and reverses
481 cardiac hypertrophy. *Nat Med.* 2005;**11**:214-222.
482 13. Barrick CJ, Rojas M, Schoonhoven R, Smyth SS, Threadgill DW. Cardiac response to pressure
483 overload in 129S1/SvImJ and C57BL/6J mice: temporal- and background-dependent development
484 of concentric left ventricular hypertrophy. *Am J Physiol Heart Circ Physiol.* 2007;**292**:H2119-
485 H2130.
486 14. Rothermel BA, Berenji K, Tannous P, Kutschke W, Dey A, Nolan B, Yoo K-D, Demetroulis E,
487 Gimbel M, Cabuay B, Karimi M, Hill JA. Differential activation of stress-response signaling in
488 load-induced cardiac hypertrophy and failure. *Physiol Genomics.* 2005;**23**:18-27.
489 15. Divakaran V, Adrogue J, Ishiyama M, Entman ML, Haudek S, Sivasubramanian N, Mann DL.
490 Adaptive and maladptive effects of SMAD3 signaling in the adult heart after hemodynamic
491 pressure overloading. *Circ Heart Fail.* 2009;**2**:633-642.
492 16. Garcia-Menendez L, Karamanlidis G, Kolwicz S, Tian R. Substrain specific response to cardiac
493 pressure overload in C57BL/6 mice. *Am J Physiol Heart Circ Physiol.* 2013;**305**:H397-H402.

494 17. Richards DA, Bao W, Rambo MV, Burgert M, Jucker BM, Lenhard SC. Examining the
495 relationship between exercise tolerance and isoproterenol-based cardiac reserve in murine models
496 of heart failure. *J Appl Physiol.* 2013;**114**:1202-1210.
497 18. Gogiraju R, Xu X, Bochenek ML, Steinbrecher JH, Lehnart SE, Wenzel P, Kessel M, Zeisberg
498 EM, Dobbelstein M, Schäfer K. Endothelial p53 deletion improves angiogenesis and prevents
499 cardiac fibrosis and heart failure induced by pressure overload in mice. *J Am Heart Assoc.*
500 2015;**4**:e001770.
501 19. Okayama K, Azuma J, Dosaka N, Iekushi K, Sanada F, Kusunoki H, Iwabayashi M, Rakugi H,
502 Taniyama Y, Morishita R. Hepatocyte growth factor reduces cardiac fibrosis by inhibiting
503 endothelial-mesenchymal transition. *Hypertension.* 2012;**59**:958-965.
504 20. Suryakumar G, Kasiganesan H, Balasubramanian S, Kuppuswamy D. Lack of β3 integrin
505 signaling contributes to calpain-mediated myocardial cell loss in pressure-overloaded myocardium.
506 *J Cardiovasc Pharmacol.* 2010;**55**:567-573.
507 21. Baicu CF, Zhang Y, Van Laer AO, Renaud L, Zile MR, Bradshaw AD. Effects of the absence of
508 procollagen C-endopeptidase enhancer-2 on myocardial collagen accumulation in chronic
509 pressure overload. *Am J Physiol Heart Circ Physiol.* 2012;**303**:H234-H204.
510 22. Kilkenny C, Browne WJ, Cuthill IC, Emerson M, Altman DG. Improving bioscience research
511 reporting: the ARRIVE guidelines for reporting animal research. *PLOS Biol.* 2010;**8**:e1000412.
512 23. Wilkins BJ, Dai Y-S, Bueno OF, Parsons SA, Xu J, Plank DM, Jones F, Kimball TR, Molkentin
513 JD. Calcineurin/NFAT coupling participates in pathological, but not physiological, cardiac
514 hypertrophy. *Circ Res.* 2004;**94**:110-118.
515 24. Melleby AO, Strand ME, Romaine A, Herum KM, Skrbic B, Dahl CP, Sjaastad I, Fiane AE,
516 Filmus J, Christensen G, Lunde IG. The heparan sulfate proteoglycan Glypican-6 is upregulated
517 in the failing heart, and regulates cardiomyocyte growth through ERK1/2 signaling. *PLoS ONE.*
518 2016;**11**:e0165079.
519 25. Baumgartner H, Hung J, Bermejo J, Chambers JB, Evangelista A, Griffin BP, Iung B, Otto CM,
520 Pellikka PA, Quiñones M. Echocardiographic assessment of valve stenosis: EAE/ASE
521 recommendations for clinical practice. *J Am Soc Echocardiogr.* 2009;**22**:1-23.
522 26. Pacher P, Nagayama T, Mukhopadhyay P, Batkai S, Kass DA. Measurement of cardiac function
523 using pressure-volume conductance catheter technique in mice and rats. *Nat Protoc.* 2008;**3**:1422-
524 1434.
525 27. Finsen AV, Lunde IG, Sjaastad I, Østli EK, Lyngra M, Jarstadmarken HO, Hasic A, Nygård S,
526 Wilcox-Adelman SA, Goetinck PF, Lyberg T, Skrbic B, Florholmen G, Tønnessen T, Louch WE,
527 Djurovic S, Carlson CR, Christensen G. Syndecan-4 is essential for development of concentric
528 myocardial hypertrophy via stretch-induced activation of the calcineurin-NFAT pathway. *PLoS*
529 *ONE.* 2011;**6**:e28302.
530 28. Dirkx E, da Costa Martins PA, De Windt LJ. Regulation of fetal gene expression in heart failure.
531 *Biochim Biophys Acta Mol Basis Dis.* 2013;**1832**:2414-2424.
532 29. Baumgarten G, Knuefermann P, Kalra D, Gao F, Taffet GE, Michael L, Blackshear PJ, Carballo E,
533 Sivasubramanian N, Mann DL. Load-dependent and -independent regulation of proinflammatory
534 cytokine and cytokine receptor gene expression in the adult mammalian heart. *Circulation.*
535 2002;**105**:2192-2197.
536 30. Pibarot P, Dumesnil JG. Low-flow, low-gradient aortic stenosis with normal and depressed left
537 ventricular ejection fraction. *J Am Coll Cardiol.* 2012;**60**:1845-1853.
538 31. Alexander N, Edmondson HA, Drury DR. The production of experimental congestive heart failure
539 in rabbits. *Circ Res.* 1953;**1**:491-498.
540 32. Menard MG. Production of experimental congestive heart failure in the guinea pig. *Proc Soc Exp*
541 *Biol Med.* 1959;**102**:396-397.
542 33. Nair KG, Cutilletta AF, Zak R, Koide T, Rabinowitz M. Biochemical correlates of cardiac
543 hypertrophy. *Circ Res.* 1968;**23**:451-462.

34. Hu P, Zhang D, Swenson L, Chakrabarti G, Abel ED, Litwin SE. Minimally invasive aortic banding in mice: effects of altered cardiomyocyte insulin signaling during pressure overload. *Am J Physiol Heart Circ Physiol.* 2003;**285**:H1261-H1269.
35. Hampton C, Rosa R, Campbell B, Kennan R, Gichuru L, Ping X, Shen X, Small K, Madwed J, Lynch JJ. Early echocardiographic predictors of outcomes in the mouse transverse aortic constriction heart failure model. *J Pharmacol Toxicol Methods.* 2017;**84**:93-101.
36. Huang J, Wu J, Wang S, You J, Ye Y, Ding Z, Yang F, Wang X, Guo J, Ma L, Yuan J, Shen Y, Yang X, Sun A, Jiang H, Bu L, Backx PH, Ge J, Zou Y. Ultrasound biomicroscopy validation of a murine model of cardiac hypertrophic preconditioning: comparison with a hemodynamic assessment. *Am J Physiol Heart Circ Physiol.* 2017;**313**:H138-H148.
37. Lygate CA, Schneider JE, Hulbert K, ten Hove M, Sebag-Montefiore LM, Cassidy PJ, Clarke K, Neubauer S. Serial high resolution 3D–MRI after aorticbanding in mice: band internalization is asource of variability in the hypertrophicresponse. *Basic Res Cardiol.* 2006;**101**:8-16.
38. Skrbic B, Engebretsen KV, Strand ME, Lunde IG, Herum KM, Marstein HS, Sjaastad I, Lunde PK, Carlson CR, Christensen G, Bjornstad JL, Tonnessen T. Lack of collagen VIII reduces fibrosis and promotes early mortality and cardiac dilatation in pressure overload in mice. *Cardiovasc Res.* 2015;**106**:32-42.
39. Takahashi R, Asai T, Murakami H, Murakami R, Tsuzuki M, Numaguchi Y, Matsui H, Murohara T, Okumura K. Pressure Overload-Induced Cardiomyopathy in Heterozygous Carrier Mice of Carnitine Transporter Gene Mutation. *Hypertension.* 2007;**50**:497-502.
40. Waehre A, Halvorsen B, Yndestad A, Husberg C, Sjaastad I, Nygård S, Dahl CP, Ahmed MS, Finsen AV, Reims H, Louch WE, Hilfiker-Kleiner D, Vinge LE, Roald B, Attramadal H, Lipp M, Gullestad L, Aukrust P, Christensen G. Lack of chemokine signaling through CXCR5 causes increased mortality, ventricular dilatation and deranged matrix during cardiac pressure overload. *PLOS ONE.* 2011;**6**:e18668.
41. Liu J, Han P, Xiao Y, Liu J, Kang YJ. A novel knot method for individually measurable aortic constriction in rats. *Am J Physiol Heart Circ Physiol.* 2014;**307**:H987-H995.
42. Gomes Júnior DC, Nassar EJ, Dórea Neto FA, Lima AE, Martins Filho EF, Oriá AP. Experimental acrylonitrile butadiene styrene and polyamide evisceration implant: a rabbit clinical and histopathology study. *Arq Bras Med Vet Zootec.* 2016;**68**:1168-1176.
43. Junior DCG, Nassar EJ, de Assis F, Neto D, Estrela-Lima A, dos Santos Honsho C, Filho EFM, Oriá AP. Tissue reaction and integration of polyamide and acrylonitrile-butadiene-styrene spheres in rat subcutaneous tissue. *Rev Bras Med Vet.* 2016;**38**:93-98.
44. Bjørnstad JL, Skrbic B, Sjaastad I, Bjørnstad S, Christensen G, Tønnessen T. A mouse model of reverse cardiac remodelling following banding - debanding of the ascending aorta. *Acta Physiol.* 2012;**205**:92-102.
45. Byrne NJ, Levasseur J, Sung MM, Masson G, Boisvenue J, Young ME, Dyck JRB. Normalization of cardiac substrate utilization and left ventricular hypertrophy precede functional recovery in heart failure regression. *Cardiovasc Res.* 2016;**110**:249-257.
46. Furihata T, Kinugawa S, Takada S, Fukushima A, Takahashi M, Homma T, Masaki Y, Tsuda M, Matsumoto J, Mizushima W, Matsushima S, Yokota T, Tsutsui H. The experimental model of transition from compensated cardiac hypertrophy to failure created by transverse aortic constriction in mice. *IJC Heart Vasc.* 2016;**11**:24-28.
47. Houser SR, Margulies KB, Murphy AM, Spinale FG, Francis GS, Prabhu SD, Rockman HA, Kass DA, Molkentin JD, Sussman MA, Koch WJ. Animal models of heart failure. *Circ Res.* 2012;**111**:131-150.
48. Horgan S, Watson C, Glezeva N, Baugh J. Murine models of diastolic dysfunction and heart failure with preserved ejection fraction. *J Card Fail.* 2014;**20**:984-995.
49. Ling ET, Bold AJd. An improved method for the production of experimental congestive heart failure in the guinea-pig. *Lab Anim.* 1976;**10**:285-289.

50. Schunkert H, Dzau VJ, Tang SS, Hirsch AT, Apstein CS, Lorell BH. Increased rat cardiac angiotensin converting enzyme activity and mRNA expression in pressure overload left ventricular hypertrophy. Effects on coronary resistance, contractility, and relaxation. *J Clin Invest.* 1990;**86**:1913-1920.
51. Zhang X, Javan H, Li L, Szucsik A, Zhang R, Deng Y, Selzman CH. A modified murine model for the study of reverse cardiac remodelling. *Exp Clin Cardiol.* 2013;**18**:e115-e117.
52. Javan H, Szuscik AM, Li L, Schaaf CL, Salama ME, Selzman CH. Cardiomyocyte p65 NF-κB is necessary for compensatory adaptation to pressure-overload. *Circ Heart fail.* 2015;**8**:109-118.
53. Koentges C, Pepin ME, Müsse C, Pfeil K, Alvarez SVV, Hoppe N, Hoffmann MM, Odening KE, Sossalla S, Zirlik A, Hein L, Bode C, Wende AR, Bugger H. Gene expression analysis to identify mechanisms underlying heart failure susceptibility in mice and humans. *Basic Res Cardiol.* 2017;**113**:8.

620 **Figure legends**

621

622 **Figure 1. Detailed description of o-ring aortic banding (ORAB)**

623 Sutures attached to the two sides of the o-ring are placed on opposite sides of the aorta (**A**). By pulling the
624 sutures in opposite directions the o-ring is opened and can be placed around the aorta (**B**). Two sets of
625 overhand knots are tied on each side of the o-ring to close it and thereby constrict the aorta (**C**). Excess
626 suture is cut and the thoracic cavity can be evacuated (**D**).

627

628 **Figure 2. ORAB results in reproducible and graded myocardial hypertrophy**

629 **A**, Representative echocardiographic M-mode tracings of mice two weeks after o-ring aortic banding
630 (ORAB) or sham operation, and echocardiographic measurements of left ventricular posterior wall
631 (LVPW) and interventricular septum (IVS) in diastole (d), respectively, at baseline (0), 1, 2, 8 and 20
632 weeks post-surgery. Sham-operated mice had a nitrile rubber insert (sham rub) and o-rings had inner
633 diameters of 0.71, 0.66 or 0.61 mm. n=5-7 at baseline, n=7-10 at all other time points. **B**, LV mass
634 calculated from MRI post-ORAB (n=6 at baseline, n=5-6 at all other time points). **C**, Post-mortem heart
635 weights at 2, 4 and 20 weeks post-ORAB (n=7-19). LV mass and heart weight were normalized to tibia
636 length. Repeated measures two-way ANOVA with Tukey's post-hoc test (A-B) and one-way ANOVA
637 with Bonferroni post-hoc test (C) were used for statistical analysis.

638

639 **Figure 3. ORAB results in reproducible and graded cardiac dilatation and dysfunction**

640 **A**, Left ventricular ejection fraction (LVEF**)**, **B**, LV end-diastolic volume (LVEDV), **C,** LV inner diameter
641 (LVID) in diastole (d), **D**, LV lumen length, and **E**, left atrial diameter (LAD) in sham-operated with
642 nitrile rubber insert (sham rub) or o-ring aortic banded (ORAB) mice at baseline (0), 1, 2, 8 and 20 weeks
643 post-surgery. O-rings had inner diameters 0.71, 0.66 and 0.61 mm. LVEF, LVEDV and LV lumen length
644 were assayed by MRI (n=6 at baseline, n=5-6 at all other time points), whereas LVIDd and LAD were

645 measured by echocardiography (n=5-7 at baseline, n=7-10 at all other time points). **F**, Post-mortem lung
646 weights at 2, 4 and 20 weeks post-ORAB (n=7-19). Lung weight was normalized to tibia length. Repeated
647 measures two-way ANOVA with Tukey's post-hoc test (A-E) and one-way ANOVA with Bonferroni or
648 Dunnet's C post-hoc test (F) were used for statistical analysis.
649
650 **Figure 4. Signature molecules of cardiac remodeling and failure show a graded expression profile to**
651 **ORAB**
652 Relative left ventricular (LV) mRNA levels of *Nppa*, *Nppb*, *Acta1*, *Myh7* and *Myh6* in sham-operated with
653 nitrile rubber insert (sham rub) or o-ring aortic banded (ORAB) mice at 2 (**A**), 4 (**B**), and 20 weeks (**C**)
654 post-surgery (n=7-19). O-rings had inner diameters of 0.71, 0.66 and 0.61 mm. One-way ANOVA with
655 Bonferroni or Dunnet's C post-hoc test was used for statistical analysis.
656
657 **Figure 5. Signature molecules of fibrosis show a graded expression profile to ORAB**
658 Relative left ventricular (LV) mRNA levels of *Col1a2*, *Col3a1*, *Lox*, *Ctgf* and *Tgfb1* in sham-operated
659 with nitrile rubber insert (sham rub) or o-ring aortic banded (ORAB) mice at 2 (**A**), 4 (**B**) and 20 weeks (**C**)
660 post-surgery (n=7-19). O-rings had inner diameters of 0.71, 0.66 and 0.61 mm. One-way ANOVA with
661 Bonferroni or Dunnet's C post-hoc test was used for statistical analysis.
662
663 **Figure 6. ORAB induces a graded fibrotic remodeling**
664 **A**, Representative images of whole mid-ventricular sections and 10X magnification of the region
665 contained within the black box stained with Masson's trichrome staining for collagen at 2 weeks after o-
666 ring aortic banding (ORAB) or sham operation with nitrile rubber insert (sham rub). O-rings had inner
667 diameters of 0.71, 0.66 and 0.61 mm. Scale bar whole heart, 2 mm; 10X magnification, 0.2 mm. **B**,
668 Quantification of left ventricular (LV) fibrosis (% of area of mid-ventricular section) 2, 4 and 20 weeks
669 post-surgery (n=4-19). **C**, Relative LV *Acta2* mRNA levels (n=7-10) and representative immunoblot and
670 quantification of LV α-smooth muscle actin (α-SMA) protein (n=6) 2 weeks post-surgery. Coomassie

671 brilliant blue was assayed for protein loading control. One-way ANOVA with Bonferroni or Dunnet's C
672 post-hoc test was used for statistical analysis.
673
674 **Figure 7. ORAB activates central cardiac remodeling signaling pathways and pro-inflammatory**
675 **gene expression**
676 **A**, Representative immunoblots and relative left ventricular (LV) protein levels of phospho-ERK 1/2
677 (pERK1/2), ERK1/2, pAKT, AKT, pp38 and p38 in sham-operated with nitrile rubber insert (sham rub) or
678 o-ring aortic banded (ORAB) C57BL/6J mice 2 weeks post-surgery (n=6). O-rings had inner diameters of
679 0.71, 0.66 and 0.61 mm. **B**, Relative NFAT-luciferase activity and LV weight (LVW) in FVB/N NFAT-
680 luc mice at 2 weeks post-surgery (n=7-10). **C**, Relative LV *Rcan1.4* mRNA levels in C57BL/6J mice 2
681 weeks post-ORAB (n=7-10). **D**, Relative LV mRNA levels of *Tnf*, *Il1b*, *Il18* and *Il6* in C57BL/6J mice 2
682 weeks post-ORAB (n=7-10). Coomassie brilliant blue was assayed for protein loading control. LVW was
683 normalized to tibia length. One-way ANOVA with Bonferroni or Dunnet's C post-hoc test was used for
684 statistical analysis.

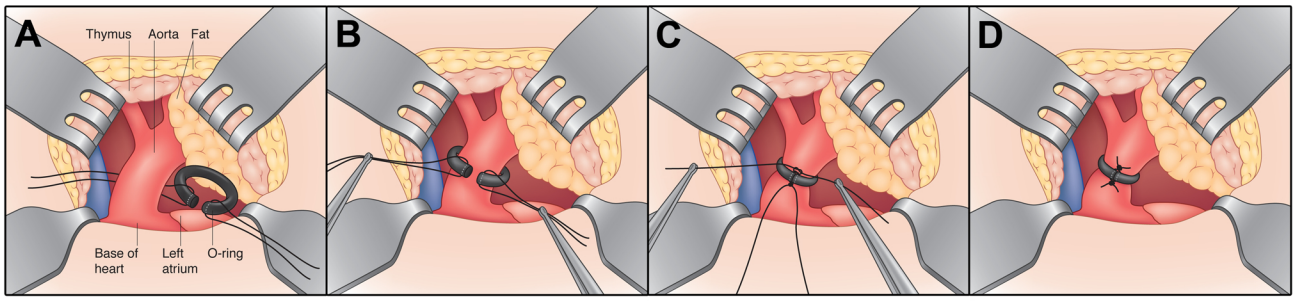

Figure 1

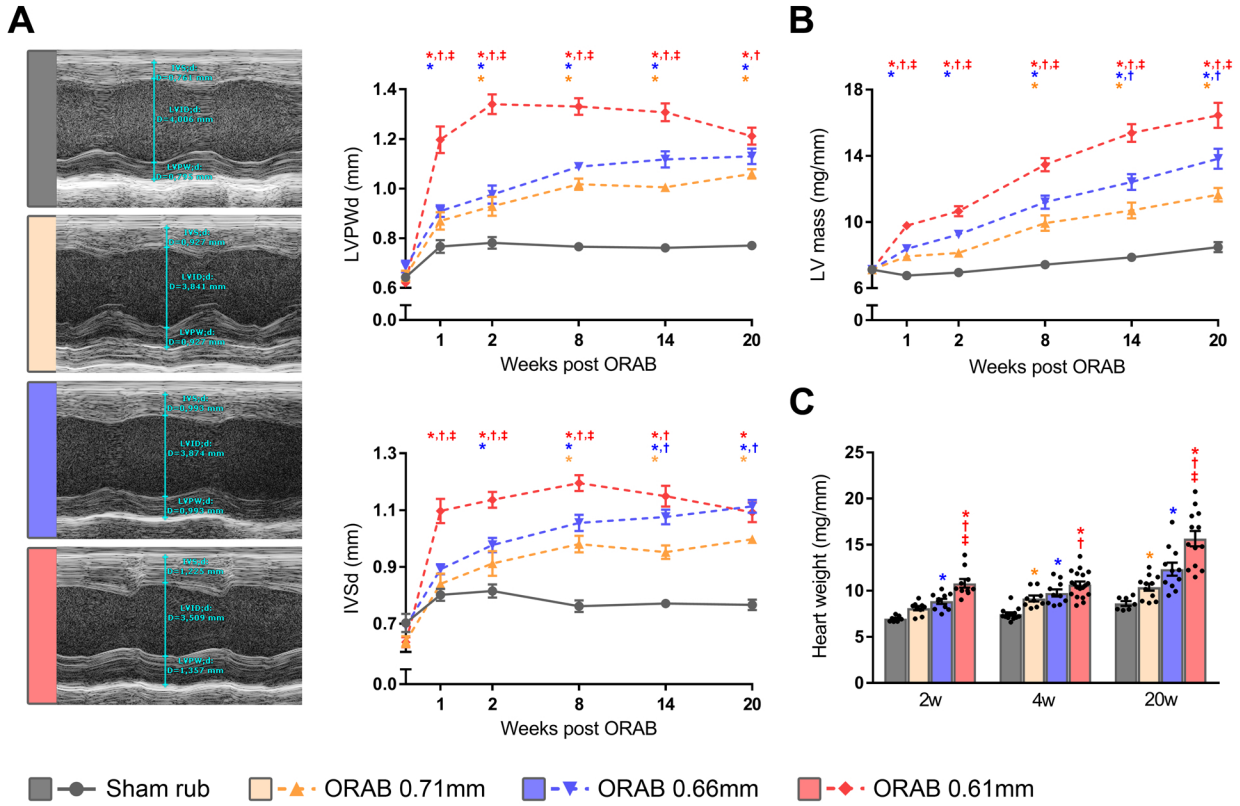
A
B
C
LVPWd (mm)
LV mass (mg/mm)
IVSd (mm)
Heart weight (mg/mm)
Weeks post ORAB
2w
4w
20w
Sham rub
ORAB 0.71mm
ORAB 0.66mm
ORAB 0.61mm

Figure 2

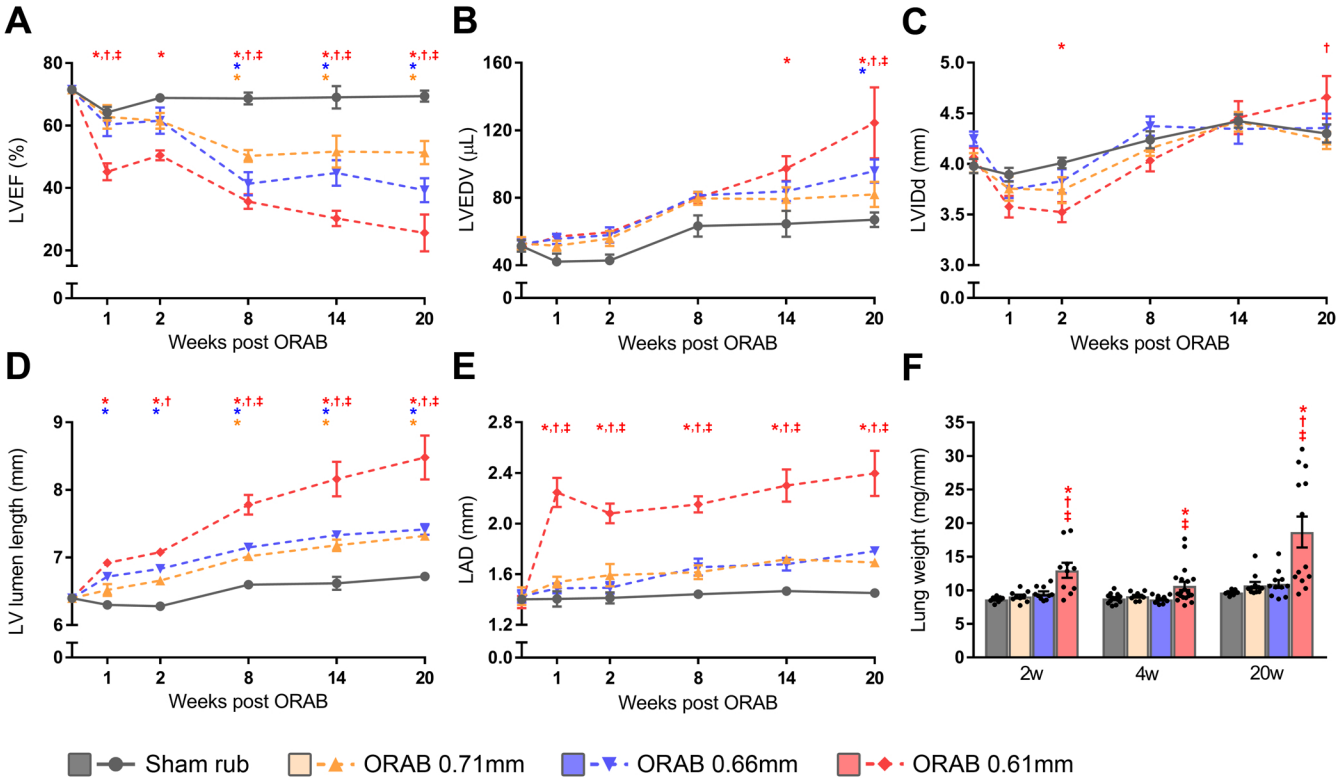
A
LVEF (%)
Weeks post ORAB
B
LVEDV (µL)
Weeks post ORAB
C
LVIDd (mm)
Weeks post ORAB
D
LV lumen length (mm)
Weeks post ORAB
E
LAD (mm)
Weeks post ORAB
F
Lung weight (mg/mm)
2w
4w
20w
Sham rub
ORAB 0.71mm
ORAB 0.66mm
ORAB 0.61mm

Figure 3

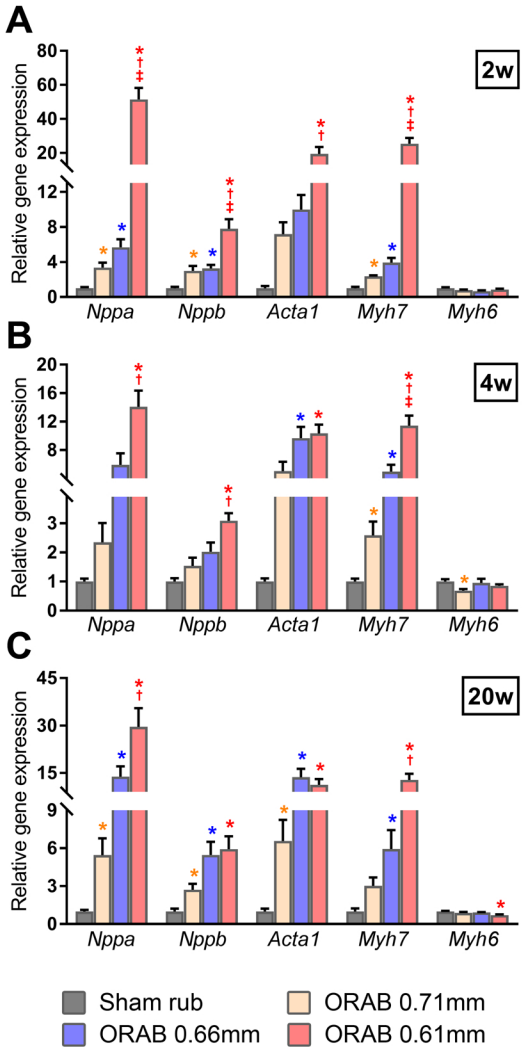
A
2w
Relative gene expression
80
60
40
20
12
8
4
0
Nppa
Nppb
Acta1
Myh7
Myh6
B
4w
Relative gene expression
20
16
12
8
3
2
1
0
Nppa
Nppb
Acta1
Myh7
Myh6
C
20w
Relative gene expression
45
30
15
9
6
3
0
Nppa
Nppb
Acta1
Myh7
Myh6
Sham rub
ORAB 0.71mm
ORAB 0.66mm
ORAB 0.61mm

Figure 4

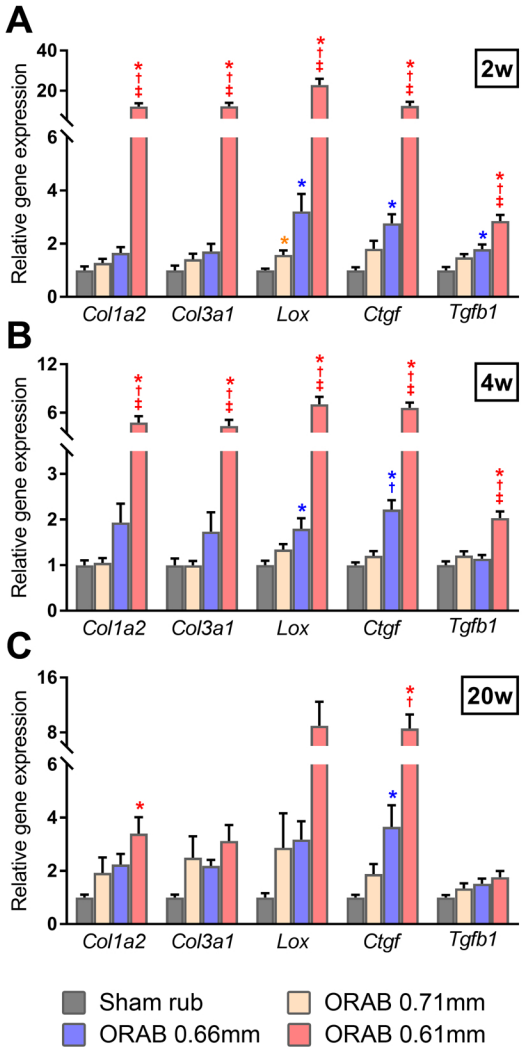
A
2w
Relative gene expression
Col1a2
Col3a1
Lox
Ctgf
Tgfb1
B
4w
C
20w
Sham rub
ORAB 0.71mm
ORAB 0.66mm
ORAB 0.61mm

Figure 5

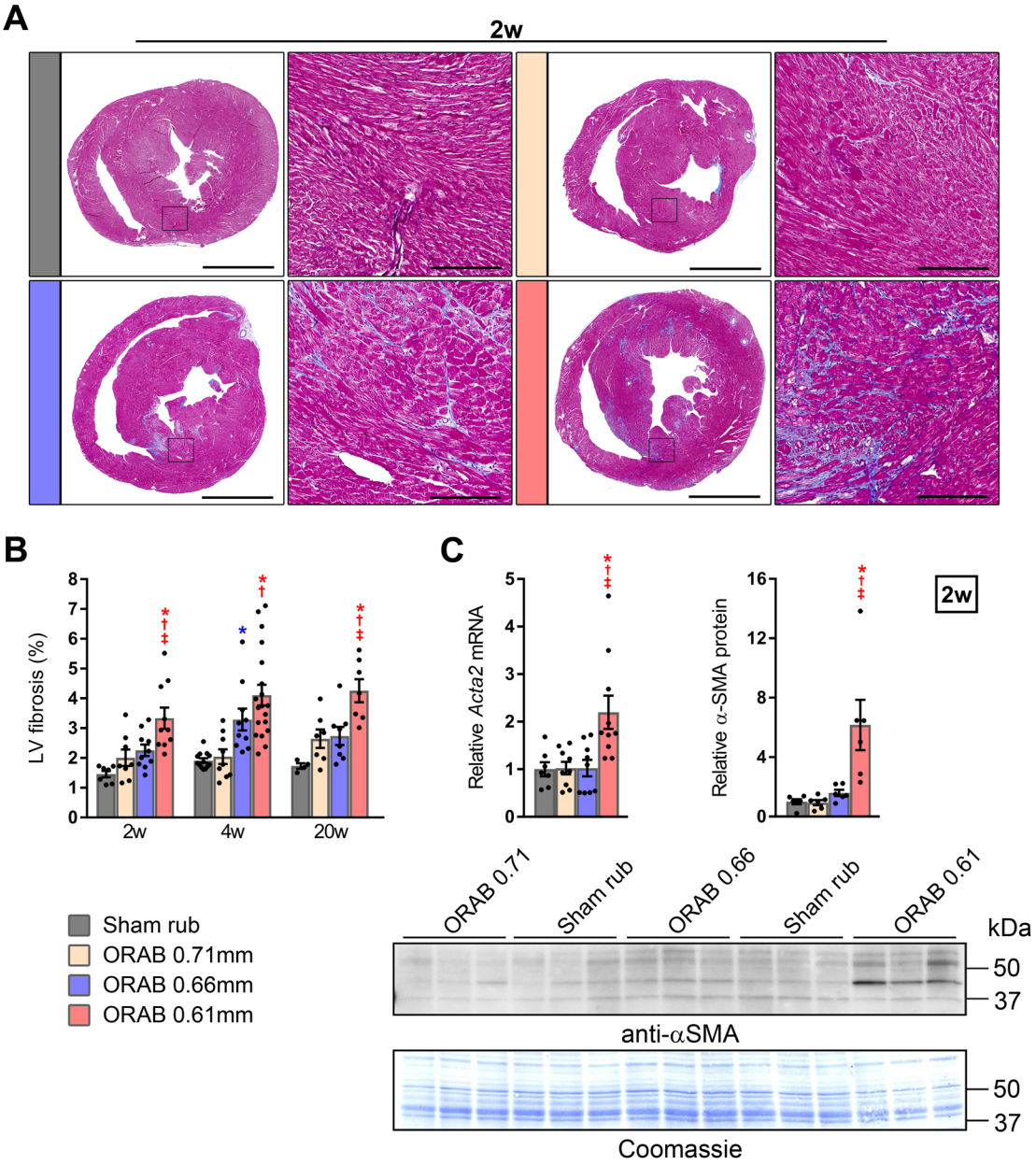
A
2w
B
LV fibrosis (%)
2w
4w
20w
Sham rub
ORAB 0.71mm
ORAB 0.66mm
ORAB 0.61mm
C
Relative Acta2 mRNA
Relative α-SMA protein
2w
ORAB 0.71
Sham rub
ORAB 0.66
Sham rub
ORAB 0.61
kDa
50
37
anti-αSMA
50
37
Coomassie

Figure 6

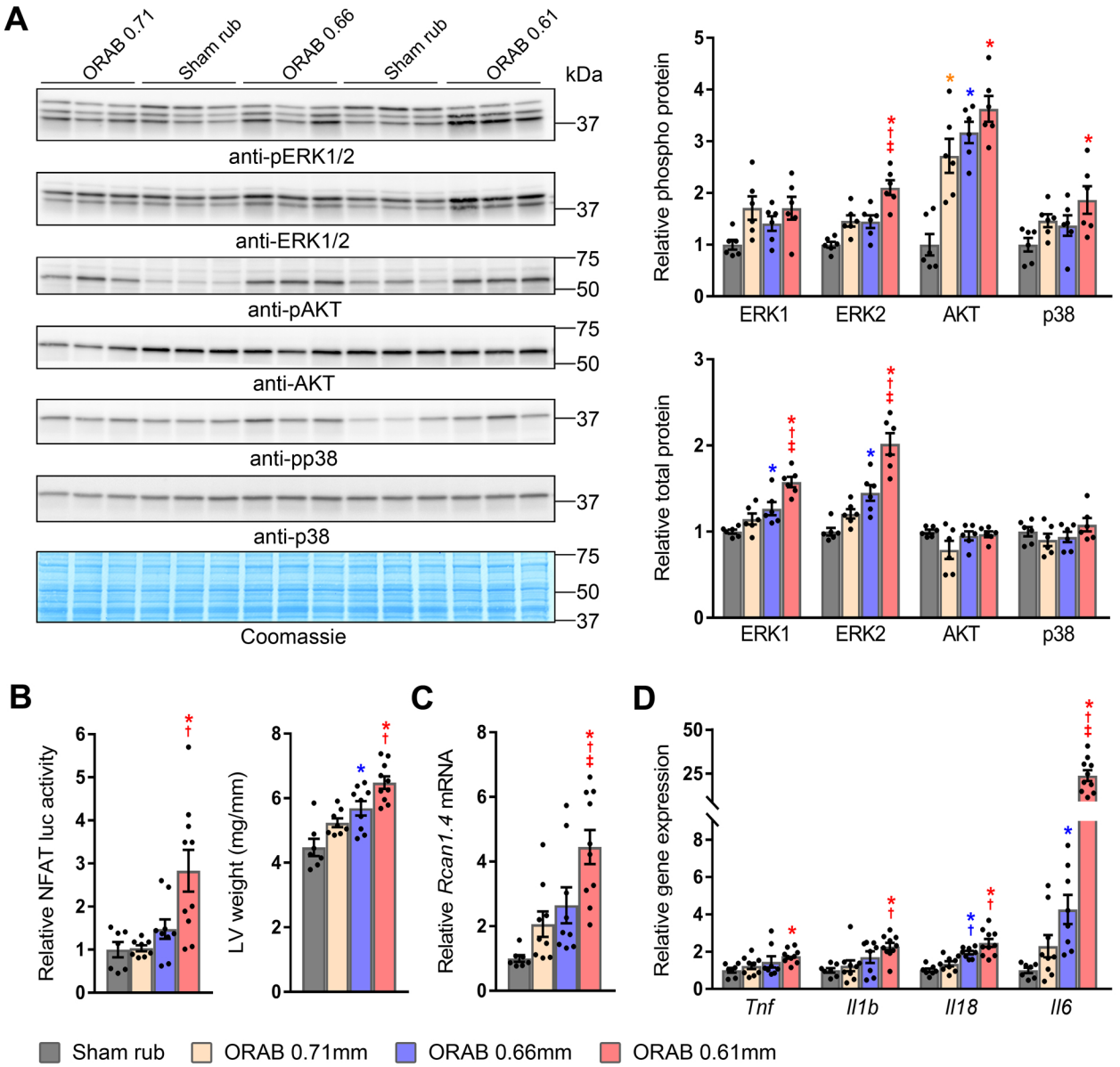
A
ORAB 0.71
Sham rub
ORAB 0.66
Sham rub
ORAB 0.61
kDa
anti-pERK1/2
anti-ERK1/2
anti-pAKT
anti-AKT
anti-pp38
anti-p38
Coomassie
Relative phospho protein
Relative total protein
ERK1
ERK2
AKT
p38
B
Relative NFAT luc activity
LV weight (mg/mm)
C
Relative Rcan1.4 mRNA
D
Relative gene expression
Tnf
Il1b
Il18
Il6
Sham rub
ORAB 0.71mm
ORAB 0.66mm
ORAB 0.61mm

Figure 7

Supplemental Material

Supplemental Methods

List of TaqMan assays used for qPCR:
Nppa (Mm01255747_g1), *Nppb* (Mm01255770_g1), *Acta1* (Mm00808218_g1), *Myh6* (Mm00440359_m1), *Myh7* (Mm00600555_m1), *Ctgf* (Mm01192932_g1), *Col1a2* (Mm00483888_m1), *Col3a1* (Mm01254476_m1), *Acta2* (Mm00725412_s1), *Lox* (Mm00495386_m1), *Rcan1* (Mm01213406_m1), *Tgfb1* (Mm01178820_m1), *Tnf* (Mm00443258_m1), *Il1b* (Mm01336189_m1), *Il18* (Mm00434225_m1), *Il6* (00446190_m1) and *Rpl32* (Mm02528467_g1). All Taqman assays were from Applied Biosystems (Foster City, CA, USA).

Protein isolation buffer:
1X PBS containing 1 % Triton X-100 (Sigma-Aldrich, St. Louis, MO, USA), 0.1 % Tween-20 (Sigma-Aldrich), protease inhibitor (Complete EDTA-free tablets, Roche Diagnostics, Oslo, Norway) and phosphatase inhibitor (PhosStop, Roche Diagnostics),

List of applied antibodies:
Anti-phospho Thr200/Tyr204 ERK1/2 (#9101, Cell Signaling Technology, Danvers, MA, USA), anti-ERK1/2 (#9102, Cell Signaling Technology), anti-phospho Ser473 AKT (#9271, Cell Signaling Technology), anti-AKT (#9272, Cell Signaling Technology), anti-phospho Thr180/Tyr182 p38 (#9211, Cell Signaling Technology), anti-p38 (#9212, Cell Signaling Technology) and anti-α-SMA (#A5228, Sigma-Aldrich). HRP-conjugated donkey-anti-rabbit (NA934, Amersham/GE HealthCare) and sheep-anti-mouse (NA931, Amersham/GE HealthCare) secondary antibodies were used for the primary antibodies.

Supplemental Figures

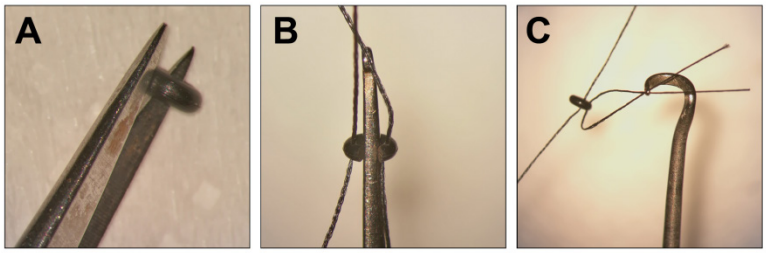

Figure S1. Preparation of o-rings for o-ring aortic banding (ORAB)
A, Opening of o-ring performed with a small pair of scissors. **B**, Placement of sutures through both sides of the open o-ring. **C**, Suture thread through a hole in a modified spinal cord hook that is used to place the two sets of sutures on opposite sides of the aorta.

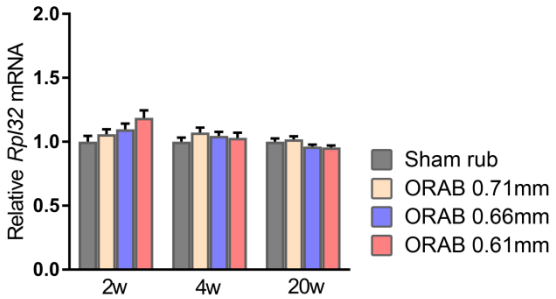

Figure S2. Assessment of reference gene *Rpl32* levels after ORAB surgery
Relative left ventricular (LV) mRNA levels of *Rpl32* in sham-operated with nitrile rubber insert (sham rub) or o-ring aortic banded (ORAB) mice at 2, 4 and 20 weeks post-surgery (n=7-19). O-rings had inner diameters of 0.71, 0.66 and 0.61 mm. One-way ANOVA with Bonferroni post-hoc test was used for statistical analysis.

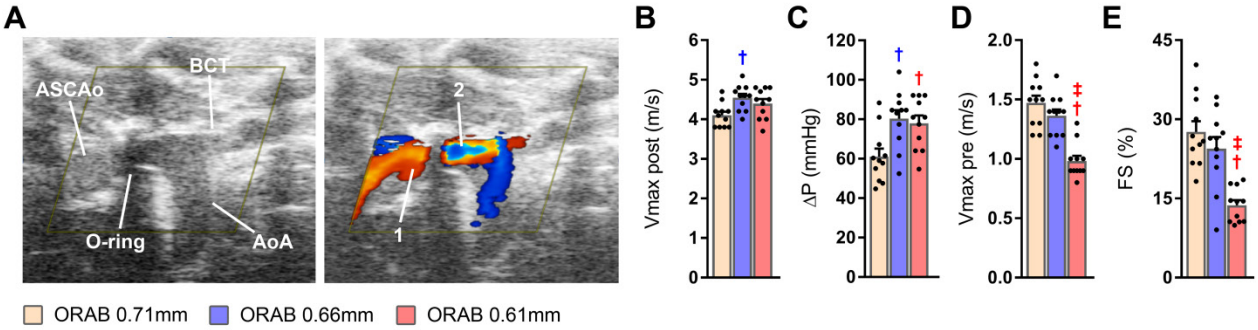

Figure S3. Assessment of stenosis-grade and cardiac function 24 hours post-ORAB
A, Regular and color Doppler echocardiograms of a mouse aorta after o-ring aortic banding (ORAB). Line 1 refers to the maximum velocity flow (Vmax) in front of the constriction (Vmax pre), whereas line 2 points to the Vmax directly after the stenosis (Vmax post). **B-E**, Echocardiographic measurements of Vmax post (**B**), calculated trans-stenotic pressure gradient (**C**), Vmax pre (**D**) and calculated fractional shortening (FS) (**E**) at 24 hours after ORAB (n=9-11). ASCAo=Ascending aorta, BCT=Brachiocephalic trunk, AoA=Aortic arch. One-way ANOVA with Bonferroni post-hoc test was used for statistical analysis († $P<0.05$ vs ORAB 0.71, ‡ $P<0.05$ vs ORAB 0.66).

Supplemental Tables

Table S1. Longitudinal echocardiographic characterization of mice subjected to ORAB

	Operation	n=	LVPWd (mm)	IVSd (mm)	LVIDd (mm)	LAD (mm)	FS (%)	Wall/ Lumen	ASCAoD (mm)	HR (bpm)	BW (g)
BL	Sham rub	5	0.70 ± 0.04	0.82 ± 0.03	3.90 ± 0.09	1.40 ± 0.03	22 ± 2	0.39 ± 0.02	1.21 ± 0.01	463 ± 22	22.9 ± 0.6
	ORAB 0.71	7	0.65 ± 0.02	0.64 ± 0.02	4.01 ± 0.10	1.43 ± 0.07	19 ± 1	0.32 ± 0.01	1.24 ± 0.03	474 ± 19	23.1 ± 0.3
	ORAB 0.66	7	0.69 ± 0.02	0.75 ± 0.02	4.22 ± 0.07	1.43 ± 0.05	18 ± 1	0.34 ± 0.01	1.21 ± 0.03	477 ± 15	22.9 ± 0.3
	ORAB 0.61	7	0.62 ± 0.01	0.64 ± 0.02	4.06 ± 0.10	1.38 ± 0.04	18 ± 2	0.31 ± 0.01	1.16 ± 0.03	463 ± 25	22.5 ± 0.3
1w	Sham rub	7	0.77 ± 0.03	0.80 ± 0.02	3.89 ± 0.07	1.41 ± 0.06	24 ± 2	0.40 ± 0.01	-	494 ± 9	-
	ORAB 0.71	8	0.87 ± 0.04	0.84 ± 0.04	3.76 ± 0.12	1.54 ± 0.04	24 ± 2	0.46 ± 0.04	-	522 ± 20	-
	ORAB 0.66	8	0.91 ± 0.02 *	0.89 ± 0.02	3.75 ± 0.09	1.48 ± 0.04	25 ± 2	0.48 ± 0.02	-	526 ± 21	-
	ORAB 0.61	10	1.20 ± 0.05 *†‡	1.10 ± 0.04 *†‡	3.58 ± 0.11	2.25 ± 0.12 *†‡	23 ± 1	0.65 ± 0.04 *†‡	-	509 ± 18	-
2w	Sham rub	7	0.78 ± 0.02	0.82 ± 0.02	4.01 ± 0.05	1.41 ± 0.04	23 ± 2	0.40 ± 0.01	-	509 ± 12	-
	ORAB 0.71	8	0.93 ± 0.04 *	0.91 ± 0.04	3.74 ± 0.13	1.59 ± 0.09	24 ± 2	0.50 ± 0.03 *	-	548 ± 19	-
	ORAB 0.66	8	0.98 ± 0.04 *	0.98 ± 0.03 *	3.83 ± 0.12	1.49 ± 0.05	24 ± 2	0.52 ± 0.03 *	-	542 ± 17	-
	ORAB 0.61	10	1.34 ± 0.04 *†‡	1.14 ± 0.03 *†‡	3.52 ± 0.10 *	2.08 ± 0.08 *†‡	25 ± 2	0.71 ± 0.03 *†‡	-	526 ± 20	-
4w	Sham rub		-	-	-	-	-	-	-	-	26.0 ± 0.7
	ORAB 0.71	8	1.00 ± 0.03	1.00 ± 0.04	3.71 ± 0.18	1.62 ± 0.04	27 ± 2	0.56 ± 0.05	-	533 ± 22	26.6 ± 0.5
	ORAB 0.66	8	1.06 ± 0.03	1.06 ± 0.02	3.79 ± 0.05	1.54 ± 0.03	25 ± 2	0.56 ± 0.01	-	535 ± 16	25.9 ± 0.5
	ORAB 0.61	10	1.38 ± 0.04 †‡	1.21 ± 0.04 †‡	3.64 ± 0.12	1.95 ± 0.06 †‡	23 ± 1	0.72 ± 0.04 †‡	-	528 ± 13	26.3 ± 0.4
8w	Sham rub	7	0.77 ± 0.01	0.76 ± 0.02	4.24 ± 0.08	1.44 ± 0.02	25 ± 3	0.36 ± 0.01	-	541 ± 21	28.4 ± 0.8
	ORAB 0.71	8	1.02 ± 0.02 *	0.98 ± 0.03 *	4.16 ± 0.08	1.62 ± 0.05	24 ± 1	0.48 ± 0.01 *	-	544 ± 11	28.6 ± 0.6
	ORAB 0.66	8	1.09 ± 0.02 *	1.06 ± 0.03 *	4.37 ± 0.09	1.66 ± 0.06	23 ± 2	0.49 ± 0.01 *	-	531 ± 18	28.5 ± 0.5
	ORAB 0.61	10	1.33 ± 0.03 *†‡	1.20 ± 0.03 *†‡	4.03 ± 0.11	2.15 ± 0.07 *†‡	19 ± 1 *	0.63 ± 0.02 *†‡	-	543 ± 14	29.0 ± 0.4
14w	Sham rub	7	0.76 ± 0.01	0.77 ± 0.01	4.42 ± 0.07	1.47 ± 0.02	21 ± 1	0.35 ± 0.01	-	468 ± 14	31.2 ± 0.9
	ORAB 0.71	8	1.01 ± 0.01 *	0.95 ± 0.02 *	4.42 ± 0.10	1.72 ± 0.03	21 ± 1	0.44 ± 0.01 *	-	503 ± 15	30.7 ± 0.7
	ORAB 0.66	8	1.12 ± 0.03 *	1.08 ± 0.03 *†	4.35 ± 0.15	1.70 ± 0.05	20 ± 2	0.51 ± 0.03 *	-	550 ± 13 *	31.0 ± 0.6
	ORAB 0.61	10	1.31 ± 0.04 *†‡	1.15 ± 0.04 *†	4.46 ± 0.16	2.30 ± 0.13 *†‡	17 ± 1	0.56 ± 0.03 *†	-	517 ± 10	30.8 ± 0.4
20w	Sham rub	7	0.77 ± 0.01	0.77 ± 0.02	4.30 ± 0.09	1.45 ± 0.03	23 ± 2	0.36 ± 0.01	-	511 ± 10	33.1 ± 1.1
	ORAB 0.71	8	1.06 ± 0.02 *	1.00 ± 0.01 *	4.23 ± 0.08	1.69 ± 0.04	22 ± 1	0.49 ± 0.01 *	-	527 ± 15	32.5 ± 0.9
	ORAB 0.66	8	1.13 ± 0.03 *	1.11 ± 0.02 *†	4.35 ± 0.14	1.79 ± 0.03	18 ± 1	0.52 ± 0.02 *	-	549 ± 18	32.8 ± 0.6
	ORAB 0.61	10	1.21 ± 0.03 *†	1.09 ± 0.03 *	4.66 ± 0.21 †	2.40 ± 0.18 *†‡	13 ± 1 *†	0.51 ± 0.03 *	-	528 ± 23	31.4 ± 0.9

M-mode echocardiographic measurements of cardiac dimensions and function in sham-operated with nitrile rubber insert (sham rub) and o-ring aortic banded (ORAB) mice at baseline (BL), 1, 2, 4, 8, 14 and 20 weeks after surgery. O-rings had inner diameters of 0.71 mm, 0.66 mm and 0.61 mm. Structural dimensions were measured in diastole (d). LVPW=left ventricular posterior wall, IVS= interventricular septum, LVID=left ventricular inner diameter, LAD=left atrial diameter, FS=fractional shortening, ASCAoD=ascending aorta diameter, HR=heart rate, BW=body weight. Repeated measures two-way ANOVA with Tukey's post-hoc test was used for longitudinal paired analysis, one-way ANOVA with Bonferroni post-hoc test was used for the 4 week time point (*P<0.05 vs sham rub, †P<0.05 vs ORAB 0.71, ‡P<0.05 vs ORAB 0.66).

Table S2. Longitudinal MRI characterization of mice subjected to ORAB

	Operation	n=	LVM/TL (mg/mm)	LVEDV (µL)	LVEF (%)	CO (ml/min)	LV lumen length (mm)	HR (bpm)
BL	-	6	7.13 ± 0.07	52.6 ± 3.0	72 ± 1	21.1 ± 0.8	6.40 ± 0.06	565 ± 10
1w	Sham rub	5	6.75 ± 0.11	42.2 ± 4.8	64 ± 2	14.1 ± 1.0	6.30 ± 0.05	531 ± 19
	ORAB 0.71	5	7.92 ± 0.11	51.5 ± 3.1	63 ± 4	18.8 ± 0.5 *	6.52 ± 0.09	589 ± 12
	ORAB 0.66	6	8.38 ± 0.12 *	55.6 ± 3.0	60 ± 4	19.1 ± 1.0 *	6.72 ± 0.03 *	578 ± 21
	ORAB 0.61	5	9.79 ± 0.25 *†‡	57.0 ± 2.1	45 ± 3 *†‡	15.8 ± 0.9	6.92 ± 0.07 *	617 ± 11 *
2w	Sham rub	5	6.95 ± 0.18	42.9 ± 3.5	69 ± 1	16.5 ± 1.4	6.28 ± 0.05	560 ± 4
	ORAB 0.71	5	8.13 ± 0.17	55.9 ± 4.5	61 ± 3	19.7 ± 1.6	6.66 ± 0.07	576 ± 19
	ORAB 0.66	6	9.25 ± 0.13 *	58.0 ± 4.6	62 ± 4	19.2 ± 0.8	6.83 ± 0.03 *	555 ± 27
	ORAB 0.61	5	10.66 ± 0.30 *†‡	59.6 ± 1.6	50 ± 2 *	17.9 ± 0.3	7.08 ± 0.06 *†	597 ± 10
4w	Sham rub		-	-	-	-	-	-
	ORAB 0.71	5	8.82 ± 0.20	62.2 ± 3.3	62 ± 2	21.1 ± 1.2	6.80 ± 0.05	552 ± 18
	ORAB 0.66	6	9.84 ± 0.20 †	68.4 ± 2.2	50 ± 3 †	20.3 ± 0.8	6.80 ± 0.04	601 ± 20
	ORAB 0.61	5	11.65 ± 0.12 †‡	69.3 ± 1.7	46 ± 2 †	18.9 ± 0.8	7.10 ± 0.07 †‡	597 ± 13
8w	Sham rub	5	7.42 ± 0.15	63.3 ± 6.3	69 ± 2	22.5 ± 1.4	6.60 ± 0.05	528 ± 26
	ORAB 0.71	5	9.93 ± 0.46 *	79.7 ± 3.9	50 ± 2 *	23.2 ± 1.0	7.02 ± 0.05 *	583 ± 12
	ORAB 0.66	6	11.20 ± 0.40 *	81.4 ± 2.4	41 ± 4 *	19.5 ± 0.8	7.15 ± 0.04 *	590 ± 14 *
	ORAB 0.61	5	13.46 ± 0.40 *†‡	80.0 ± 2.9	36 ± 2 *†	16.4 ± 0.9 *†	7.78 ± 0.15 *†‡	581 ± 14
14w	Sham rub	5	7.87 ± 0.19	64.6 ± 7.7	69 ± 4	22.1 ± 1.5	6.62 ± 0.10	510 ± 26
	ORAB 0.71	5	10.70 ± 0.48 *	79.2 ± 7.0	52 ± 5 *	22.6 ± 0.6	7.18 ± 0.09 *	571 ± 8
	ORAB 0.66	6	12.42 ± 0.47 *†	83.9 ± 5.8	45 ± 4 *	20.8 ± 0.7	7.33 ± 0.06 *	572 ± 12 *
	ORAB 0.61	5	15.39 ± 0.54 *†‡	97.3 ± 7.3 *	30 ± 2 *†‡	16.3 ± 0.9 *†‡	8.16 ± 0.26 *†‡	567 ± 15
20w	Sham rub	5	8.48 ± 0.30	67.0 ± 4.3	69 ± 2	23.2 ± 1.3	6.72 ± 0.04	501 ± 20
	ORAB 0.71	5	11.65 ± 0.40 *	82.0 ± 7.5	51 ± 4 *	24.7 ± 0.6	7.32 ± 0.05 *	603 ± 24 *
	ORAB 0.66	6	13.82 ± 0.61 *†	95.8 ± 7.0 *	39 ± 4 *	21.2 ± 1.1	7.42 ± 0.08 *	584 ± 6 *
	ORAB 0.61	5	16.45 ± 0.75 *†‡	124.3 ± 21.0 *†‡	26 ± 6 *†‡	15.1 ± 1.5 *†‡	8.48 ± 0.33 *†‡	559 ± 5

MRI measurements of cardiac dimensions and function in sham-operated with nitrile rubber insert (sham rub) and o-ring aortic banded (ORAB) mice at baseline (BL), 1, 2, 4, 8, 14 and 20 weeks after surgery. O-rings had inner diameters 0.71 mm, 0.66 mm and 0.61 mm. Structural dimensions were measured in diastole (d). LVM=left ventricular mass, TL=tibia length, LVEDV=left ventricular end-diastolic volume, LVEF=left ventricular ejection fraction, CO=cardiac output, HR=heart rate. Repeated measures two-way

ANOVA with Tukey's post-hoc test was used for longitudinal paired analysis, one-way ANOVA with Bonferroni post-hoc test was used for the 4 week time point (**P*<0.05 vs sham rub, †*P*<0.05 vs ORAB 0.71, ‡*P*<0.05 vs ORAB 0.66).

Table S3. Diastolic function of ORAB 0.66mm mice

	Sham rub			ORAB 0.66			
n=		8			12		
LVM/TL (mg/mm)	8.30	±	0.26	12.4	±	0.41	*
LVEF (%)	67	±	1	44	±	3	*
LVEDV (µL)	71.7	±	4.20	87.8	±	4.60	*
EDPVR	0.07	±	0.004	0.12	±	0.004	*

MRI measurements of structural and functional cardiac parameters and calculated end-diastolic pressure-volume relationship (EDPVR) based on left ventricular catheterization in sham-operated with nitrile rubber insert (sham rub) or o-ring 0.66 mm aortic banded (ORAB 0.66) mice at 12 weeks post-surgery. LVM=left ventricular mass, TL=tibia length, LVEF=left ventricular ejection fraction, LVEDV=left ventricular end-diastolic volume. Student's *t*-test was used for statistical analysis (**P*<0.05 vs sham rub).

Table S4. Inter-operator comparison of ORAB-operated animals

	Sham rub			#1 ORAB 0.61				#2 ORAB 0.61			
Post-mortem organ weights											
n=		13			19				6		
HW/TL (mg/mm)	7.48	±	0.18	10.68	±	0.32	*	10.53	±	0.79	*
LW/TL (mg/mm)	8.78	±	0.21	10.66	±	0.61	*	9.59	±	0.18	*
BW (g)	26.3	±	0.5	26.9	±	0.4		27.0	±	0.7	
LV mRNA expression											
n=		13			19				6		
Nppa/*Rpl32*	1.00	±	0.12	14.08	±	2.28	*	15.56	±	2.57	*
Nppb/*Rpl32*	1.00	±	0.13	3.08	±	0.26	*	2.80	±	0.22	*
Acta1/*Rpl32*	1.00	±	0.16	10.34	±	1.22	*	13.66	±	2.33	*
Myh6/*Rpl32*	1.00	±	0.06	0.85	±	0.05		0.87	±	0.07	
Myh7/*Rpl32*	1.00	±	0.11	11.43	±	1.40	*	11.88	±	1.50	*
Col1a2/*Rpl32*	1.00	±	0.08	4.75	±	0.80	*	4.19	±	0.43	*
Col3a1/*Rpl32*	1.00	±	0.10	4.32	±	0.78	*	3.52	±	0.29	*
Rpl32	1.00	±	0.02	1.03	±	0.04		0.88	±	0.04	
Echocardiography											
n=		9			18				6		
LVPWd (mm)	0.77	±	0.02	1.25	±	0.03	*	1.20	±	0.05	*
IVSd (mm)	0.79	±	0.03	1.18	±	0.03	*	1.16	±	0.04	*
LVIDd (mm)	4.13	±	0.08	3.73	±	0.12		3.85	±	0.20	
LAD (mm)	1.37	±	0.02	1.92	±	0.07	*	1.94	±	0.06	*
FS (%)	23.9	±	0.9	22.2	±	1.0		23.6	±	0.4	
Wall/Lumen	0.38	±	0.02	0.67	±	0.03	*	0.62	±	0.05	*
HR (bpm)	528	±	14	514	±	14		511	±	21	

Post-mortem heart weight (HW) and lung weight (LW) normalized to tibia length (TL), post-mortem body weight and relative mRNA levels of hypertrophy and fibrosis-related genes normalized to *Rpl32* mRNA in sham-operated animals with nitrile rubber insert (sham rub) and 0.61 mm inner diameter o-ring aortic banded (ORAB) mice operated by two individual surgeons (#1 and #2) at 4 weeks after surgery. M-mode echocardiographic measurements of cardiac dimensions and function were acquired before tissue harvest. Structural dimensions were measured in diastole (d). LVPW=left ventricular posterior wall, LVID=left ventricular inner diameter, IVS= interventricular septum, LAD=left atrial diameter, FS=fractional shortening, HR=heart rate. One-way ANOVA with Bonferroni or Dunnet's C post-hoc test was used for statistical analysis (*P<0.05 vs sham rub).

Table S5. Assessment of nitrile rubber effects on structural and functional cardiac parameters in sham-operated mice

	BL		2w		8w		20w	
	Sham rub	Sham	Sham rub	Sham	Sham rub	Sham	Sham rub	Sham
Echocardiography								
n=	5	5	7	5	7	5	7	5
LVPWd (mm)	0.64 ± 0.02	0.68 ± 0.03	0.78 ± 0.02	0.79 ± 0.04	0.77 ± 0.01	0.74 ± 0.01	0.77 ± 0.01	0.77 ± 0.01
IVSd (mm)	0.70 ± 0.03	0.63 ± 0.03	0.82 ± 0.02	0.79 ± 0.04	0.76 ± 0.02	0.76 ± 0.03	0.77 ± 0.02	0.78 ± 0.01
LVIDd (mm)	3.98 ± 0.07	3.96 ± 0.15	4.01 ± 0.05	3.96 ± 0.11	4.24 ± 0.08	4.20 ± 0.12	4.30 ± 0.09	4.24 ± 0.16
LAD (mm)	1.40 ± 0.03	1.28 ± 0.06	1.41 ± 0.04	1.37 ± 0.06	1.44 ± 0.02	1.44 ± 0.03	1.45 ± 0.03	1.46 ± 0.02
FS (%)	20 ± 1	18 ± 1	23 ± 2	19 ± 2	25 ± 3	22 ± 1	23 ± 2	22 ± 2
Wall/Lumen	0.34 ± 0.01	0.33 ± 0.02	0.40 ± 0.01	0.40 ± 0.02	0.36 ± 0.01	0.36 ± 0.01	0.36 ± 0.01	0.37 ± 0.01
HR (bpm)	463 ± 21	462 ± 8	509 ± 12	445 ± 21 *	541 ± 21	494 ± 20	511 ± 10	498 ± 16
MRI								
n=	6	-	5	6	5	6	5	6
LVM/TL (mg/mm)	7.13 ± 0.07	-	6.75 ± 0.12	6.76 ± 0.13	7.42 ± 0.15	7.50 ± 0.18	8.48 ± 0.31	8.39 ± 0.24
LVEDV (µL)	52.6 ± 3.0	-	42.9 ± 3.5	53.6 ± 4.7	63.3 ± 6.3	67.8 ± 3.9	67.0 ± 4.3	61.9 ± 5.9
LVEF (%)	72 ± 1	-	69 ± 1	62 ± 3	69 ± 2	64 ± 2	69 ± 2	70 ± 2
CO (mL/min)	21.1 ± 0.8	-	16.5 ± 1.4	18.1 ± 0.8	22.5 ± 1.4	21.2 ± 18.6	23.2 ± 1.3	23.8 ± 2.1
LV lumen length (mm)	6.40 ± 0.06	-	6.28 ± 0.05	6.38 ± 0.03	6.60 ± 0.05	6.63 ± 0.04	6.72 ± 0.04	6.77 ± 0.06
HR (bpm)	565 ± 10	-	559 ± 4	558 ± 12	528 ± 26	492 ± 1	501 ± 20	554 ± 16

M-mode echocardiographic and MRI measurements of cardiac dimensions and functional parameters in sham-operated mice, with (sham rub) and without (sham) nitrile rubber insert, at baseline (BL), 2, 8 and 20 weeks after surgery. Structural dimensions were measured in diastole (d). LVPW=left ventricular posterior wall, IVS= interventricular septum, LVID=left ventricular inner diameter, LAD=left atrial diameter, FS=fractional shortening, HR=heart rate, LVM=left ventricular mass, TL=tibia length, LVEDV=left ventricular end-diastolic volume, LVEF=left ventricular ejection fraction, CO=cardiac output. Repeated measures two-way ANOVA with Sidak's post-hoc test was used for statistical analysis (*P<0.05 vs sham rub).

Table S6. Post-mortem assessment of nitrile rubber effects in sham-operated mice

	2 Weeks						20 Weeks						
C57BL/6J mice	Sham rub			Sham			Sham rub			Sham			
Post-mortem organ weights													
n=		7			7			7			7		
HW/TL (mg/mm)	6.96	±	0.12	7.46	±	0.31	8.63	±	0.26	8.23	±	0.24	
LW/TL (mg/mm)	8.64	±	0.17	8.73	±	0.18	9.66	±	0.15	9.54	±	0.20	
BW (g)	26.4	±	0.5	25.3	±	0.5	33.1	±	1.1	32.9	±	0.8	
LV mRNA expression													
n=		7			7			7			7		
Nppa/*Rpl32*	1.00	±	0.13	1.11	±	0.10	1.00	±	0.13	0.96	±	0.31	
Nppb/*Rpl32*	1.00	±	0.15	1.50	±	0.23	1.00	±	0.22	0.89	±	0.20	
Acta1/*Rpl32*	1.00	±	0.25	1.26	±	0.38	1.00	±	0.23	0.74	±	0.20	
Myh6/*Rpl32*	1.00	±	0.11	0.91	±	0.13	1.00	±	0.05	0.92	±	0.06	
Myh7/*Rpl32*	1.00	±	0.15	0.94	±	0.06	1.00	±	0.24	0.71	±	0.10	
Col1a2/*Rpl32*	1.00	±	0.15	1.03	±	0.15	1.00	±	0.11	0.74	±	0.07	
Col3a1/*Rpl32*	1.00	±	0.18	0.94	±	0.11	1.00	±	0.11	0.82	±	0.09	
Acta2/*Rpl32*	1.00	±	0.15	1.20	±	0.17	-			-			
Lox/*Rpl32*	1.00	±	0.06	1.20	±	0.08	1.00	±	0.16	0.69	±	0.08	
Ctgf/*Rpl32*	1.00	±	0.12	1.02	±	0.16	1.00	±	0.10	0.71	±	0.07	*
Tgfb1/*Rpl32*	1.00	±	0.12	1.25	±	0.09	1.00	±	0.09	0.84	±	0.12	
Rcan1.4/*Rpl32*	1.00	±	0.10	1.53	±	0.27	-			-			
Rpl32	1.00	±	0.05	1.00	±	0.05	1.00	±	0.03	0.98	±	0.03	
Histology													
n=		7			7			4			4		
LV fibrosis (%)	1.46	±	0.11	1.87	±	0.17	1.73	±	0.09	1.99	±	0.30	
FVB/N NFAT-luc mice	Sham rub			Sham									
n=		7			7								
LVW/TL (mg/mm)	4.48	±	0.27	4.38	±	0.15	-			-			
BW (g)	25.6	±	1.4	25.6	±	1.0	-			-			
NFAT-luc activity	1.00	±	0.18	0.81	±	0.13	-			-			

Post-mortem heart weight (HW) and lung weight (LW) normalized to tibia length (TL), post-mortem body weight (BW), relative left ventricle (LV) mRNA levels of remodeling- and fibrosis-related genes normalized to *Rpl32* mRNA, and LV fibrosis from Masson's trichrome stained mid-ventricular sections in sham-operated C57BL/6J mice, with (sham rub) and without (sham) nitrile rubber insert, at 2 and 20 weeks after surgery. Post-mortem LV weight (LVW) normalized to TL, post-mortem BW and relative NFAT luciferase (NFAT-luc) activity in sham rub and sham-operated FVB/N NFAT-luc mice at 2 weeks after surgery. Student's *t*-test was used for statistical analysis (*P<0.05 vs sham rub).